NANO LETTERS

pubs.acs.org/NanoLett

Letter

Ultra-photostable DNA FluoroCubes: Mechanism of Photostability and Compatibility with FRET and Dark Quenching

Aaron T. Blanchard, Zi Li, Elizabeth C. Duran, Catherine E. Scull, J. Damon Hoff, Keenan R. Wright, Victor Pan, and Nils G. Walter*

Cite This: *Nano Lett.* 2022, 22, 6235−6244

Read Online

ACCESS | Metrics & More | Article Recommendations | Supporting Information

ABSTRACT: DNA-based FluoroCubes were recently developed as a solution to photobleaching, a ubiquitous limitation of fluorescence microscopy (Niekamp; Stuurman; Vale *Nature Methods*, **2020**). FluoroCubes, that is, compact ∼4 × 4 × 5.4 nm^3 four-helix bundles coupled to ≤6 fluorescent dyes, remain fluorescent up to ∼50× longer than single dyes and emit up to ∼40× as many photons. The current work answers two important questions about the FluoroCubes. First, what is the mechanism by which photostability is enhanced? Second, are FluoroCubes compatible with Förster resonance energy transfer (FRET) and similar techniques? We use single particle photobleaching studies to show that photostability arises through interactions between the fluorophores and the four-helix DNA bundle. Supporting this, we discover that smaller ∼4 × 4 × 2.7 nm^3 FluoroCubes also confer ultraphotostability. However, we find that certain dye−dye interactions negatively impact FluoroCube performance. Accordingly, 4-dye FluoroCubes lacking these interactions perform better than 6-dye FluoroCubes. We also demonstrate that FluoroCubes are compatible with FRET and dark quenching applications.

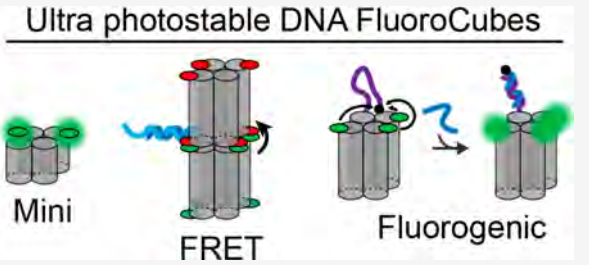

KEYWORDS: *DNA nanotechnology, fluorescence microscopy, single molecule imaging, FRET, fluorogenic probes*

Photobleaching, a process wherein fluorescent dyes irreversibly degrade due to excitation, is a nearly ubiquitous limitation in fluorescence microscopy. Photobleaching limits the observation time in temporal studies, limits spatial resolution in single molecule imaging, and biases data from fluorescent sensors designed to undergo brightness changes for biological research. A variety of solutions to this challenge have been presented, including the synthesis of photostable dyes,[1−3] the use of oxygen scavenging system (OSS)s and triplet state quenchers,[4−6] encapsulation of fluorophores within protective nanostructures,[7−11] and the creation of fluorescent nanoparticles such as quantum dots.[12] A promising recent development was the invention of ultra-photostable DNA-based FluoroCubes.[13] DNA FluoroCubes consist of four 32-nucleotide (nt) DNA strands that, when annealed together, assemble into a compact four-helix bundle with approximate dimensions of 4.0 × 4.0 × 5.6 nm^3 (Scheme 1a, Figure 1a). Three of the strands (called the A-, B-, and C-strands) are covalently labeled with fluorescent dyes at both termini, while the fourth strand (the ligand strand) presents a ligand, such as biotin, that can link the FluoroCube to a molecule of interest such as streptavidin (SA).

These compact 6-dye nanostructures are much less sensitive to photobleaching than single dyes.[13] Most notably, FluoroCubes carrying the widely used Cyanine 3 (Cy3) fluorophore were reported to exhibit a 54× increase (relative to a single Cy3 on a DNA duplex) in half-life (τ) and a 43× increase in the total photon count before photobleaching ($N_{photons}$).[13] FluoroCube-based photostability enhancement is additive with enhancements offered by both OSSs,[4,5] and dye modifications (e.g., the engineered Cy3N and ATTO 647N dyes). Combining these approaches provides total photostability that is unparalleled among organic dyes and rivals that of quantum dot nanocrystals.[13] Many questions remain unanswered about the physical underpinnings of this photostability.

FluoroCubes have enabled high precision particle tracking experiments for the long-term study of molecular motors,[13,14] and there are many additional potential application areas for FluoroCube technology. One useful feature in fluorescence is the ability to directly interrogate molecular interactions and conformations using Förster resonance energy transfer (FRET).[15−17] FRET is a process wherein energy transfers from an excited donor fluorophore to an acceptor fluorophore within a characteristic radius of typically ∼5 nm. The transferred energy is then emitted by the acceptor, resulting in emission that is red-shifted relative to the emission of the

Received: May 4, 2022
Revised: June 30, 2022
Published: July 26, 2022

https://doi.org/10.1021/acs.nanolett.2c01757
Nano Lett. 2022, 22, 6235−6244

Scheme 1. Schematics[a]

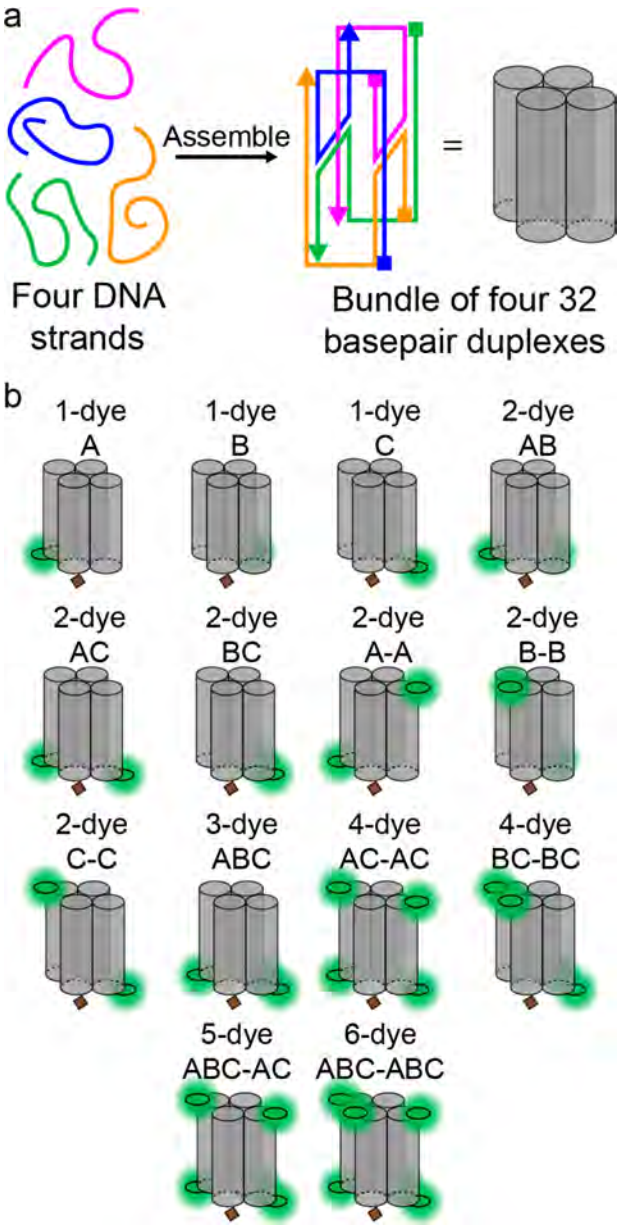

[a](a) Assembly of a DNA FluoroCube nanostructure from four 32 nucleotide DNA strands. (b) The 14 constructs studied in this work, each with dyes strategically conjugated to different combinations of DNA strand termini.

donor. FRET is used in a wide range of applications, including single molecule biophysics,[15] cellular biology,[17,18] and molecular sensing.[16,19]

A similar class of techniques utilizes dark acceptors (also called quenchers), which accept energy transfer but do not emit fluorescence. Dark quenchers are useful for conditional quenching applications, wherein donor-quencher separation produces a very large increase in fluorescence intensity for reporting on conformational changes such as DNA or RNA hybridization[20−23] or molecular tension.[24,25] In some cases, very close contact between dark quenchers and donor fluorophores can result in ground state stabilization (or "contact quenching"), wherein electronic coupling prevents donor excitation altogether.[26] We here aimed to test whether FluoroCubes are compatible with FRET and conditional quenching. To understand compatibility between these techniques and FluoroCubes, we first studied the mechanism through which FluoroCubes confer ultraphotostability.

Simple linear scaling of fluorescence with the number of dyes (n) would predict $N_{photons} \propto n$ and $\tau \propto \log(n + 1)$ (approximately, see Supporting Information Note 1). However, $\log(7) \approx 2$, which is smaller by an order of magnitude than the observed increase in τ (10−54× reported, depending on the dye[13]). Dye−dye and/or dye−DNA nanostructure interactions thus appear to enhance photostability. Interactions between dyes like Cy3 and DNA nanostructures have been shown to enhance photostability in certain contexts.[27,28] Dye−dye interactions, such as the formation of electronically coupled dye-aggregates[29−32] can also contribute to photostabilization in some cases.[33] Previous experiments[13] showed that preventing dye−dye interactions by spacing Cy3 dyes out on a larger DNA origami cube (~8 × 8 × 11 nm^3) resulted in $N_{photons}$ and τ-values that are vastly improved relative to single dsDNA-conjugated dyes, but still about 2× lower than Cy3 FluoroCubes. This led us (and others)[34] to hypothesize that both dye−dye interactions and dye−DNA interactions (i.e., interactions between individual dyes and the surface of the DNA 4-helix bundle), contribute to increased photostability.

To test this proposed model, we assembled 14 FluoroCube constructs with $1 \leq n \leq 6$ and different fluorophore positions (Scheme 1b, Figure S1, Tables S1−2). Specifically, we assembled three 1-dye constructs (1-dye A, 1-dye B, and 1-dye C, where the letter denotes which strand, the A-strand, B-strand, or C-strand, the dye is attached to), three 2-dye constructs with fluorophores on the same side of the FluoroCube (2-dye AB, 2-dye AC, and 2-dye BC), three 2-dye constructs with fluorophores on opposite sides of the FluoroCube (2-dye A-A, 2-dye B−B, and 2-dye C−C), a 3-dye construct with fluorophores all on one side of the FluoroCube (3-dye ABC), two 4-dye constructs with two fluorophores on each side (4-dye AC-AC, and 4-dye BC-BC), and 5- and 6-dye constructs (5-dye ABC-AC and 6-dye ABC-ABC).

We immobilized these constructs onto glass coverslips at low surface densities via biotin−streptavidin binding (Figure 1b). We then performed single molecule photobleaching studies of these FluoroCubes (Figures 1d-e, S2) by imaging continuously for ≥10 min using total internal reflection fluorescence (TIRF) microscopy in the presence of an OSS containing PCA/PCD and the triplet state quencher Trolox.[4,5] As previously observed,[13] FluoroCubes exhibited large fluctuations in fluorescence intensity. We also tested 1- and 2-dye FluoroCubes assembled from two oligonucleotides only, which are expected to be 50% smaller by volume than 4-strand FluoroCubes (4 × 4 × 2.7 nm^3, Figures 1c, S3). For all constructs, the average FluoroCube fluorescence intensity, $\langle I \rangle$, accurately fit a single-exponential decay model (Figures 1g and S4)

$$\langle I \rangle = I_0 \exp(-k_1 t) \quad (1)$$

where the initial intensity, I_0, and the single-dye bleach rate, k_1, are fit parameters, and t denotes the duration of laser illumination and imaging. Because n photobleaching steps must occur prior to total photobleaching, the fraction (f) of remaining bright FluoroCubes (assuming equal bleaching rates of all n dyes) can be described by

$$f = 1 - (1 - \exp(-k_1 t))^n \quad (2)$$

https://doi.org/10.1021/acs.nanolett.2c01757
Nano Lett. 2022, 22, 6235−6244

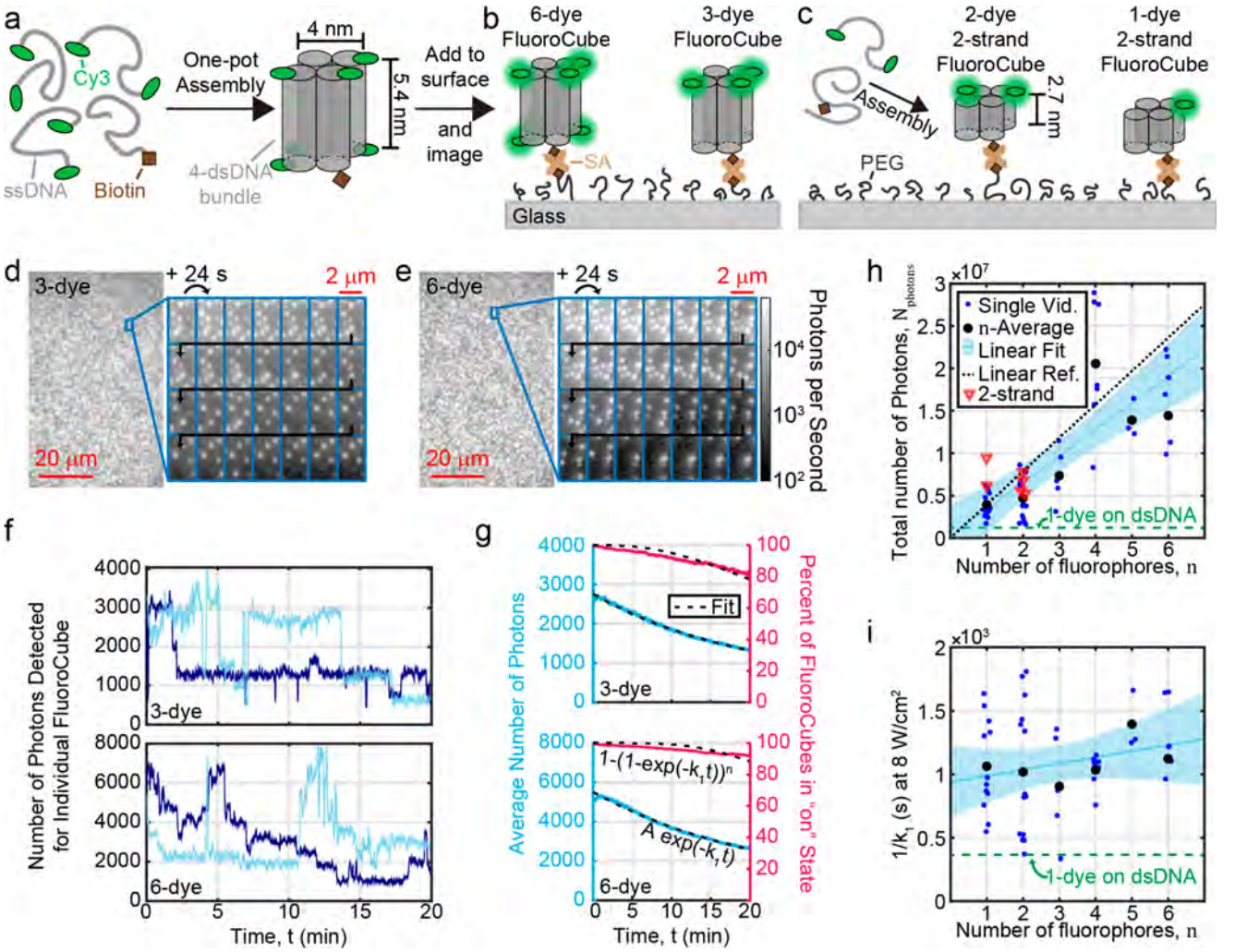

Figure 1. Cy3 FluoroCube photostability arises from interactions between fluorophores and the DNA nanostructure. (a) Schematic depiction of fluorocube assembly from four oligonucleotides. (b) Depiction of fluorocubes captured on surface via biotin−streptavidin linker. (c) Depiction of assembly and surface capture of miniature fluorocubes assembled from two strands. (d) Initial frame from video of single molecule photobleaching of 3-dye FluoroCubes. A zoomed-in region is shown for 28 frames taken at 24 s intervals throughout the video. (e) Same as d, but for 6-dye FluoroCubes. Note the logarithmic scale of the intensity scale bar applicable to panels d and e. (f) Two representative photon count versus time traces (light and dark blue curves, respectively) each for 3-dye (top) and 6-dye (bottom) FluoroCubes. (g) Average photon count (left *y*-axis scale, blue curves) and percent of unbleached FluoroCubes (right *y*-axis scale, red curves) with dashed line fits (to eqs 1 and 2, respectively) for 3-dye (top) and 6-dye (bottom) FluoroCubes. (h) Plot summarizing $N_{photons}$ versus *n* for 14 fluorocube constructs, showing roughly linear scaling. Blue curve and shading show best-fit and 95% confidence interval of the linear fit. Horizontal green dashed line indicates $N_{photons}$ for a single Cy3 dye attached to a double-stranded DNA duplex. Blue dots show best-fit values from individual videos of standard 4-strand FluoroCube photobleaching. Black dots show average of all best-fit values at a given *n*. Red triangles show best-fit values from individual videos of 2-strand FluoroCubes photobleaching. Black dotted line is a linear curve that passes through the origin and the 1-dye average value. (i) Same as h, but for $1/k_1$ (normalized to a common excitation laser power density) showing no significant correlation with n.

Fitting to both eqs 1and 2 produced similar results (Figure S5).

Although $N_{photons}$ correlated significantly with *n* ($p < 0.001$, Figure 1h), k_1 did not ($p = 0.14$, Figure 1i). In other words, the photostability of FluoroCube-bound Cy3 dyes is independent of the number of other dyes on the FluoroCube. Contrary to our original hypothesis, this finding shows that photostabilization is primarily the result of interactions between individual dyes and the DNA nanostructures they are linked to−not dye−dye interactions.

Why then did the aforementioned measurement with increased dye−dye spacings (≥8 nm) exhibit ∼2× lower τ and $N_{photons}$?[13] Upon further inspection, we found that Cy3 dyes were attached to the larger cube nanostructure via 2T overhangs, which could have partially disrupted dye−DNA interactions and thus reduced photstability.[27] Similar overhangs were not used to attach dyes to FluoroCubes, highlighting the importance and sensitivity of dye−DNA interactions in photostabilization.

Our conclusions suggest that FluoroCube size can be further reduced, so long as dye−DNA interactions are preserved. To test this hypothesis, we designed 1-dye and 2-dye FluoroCubes composed of only two strands with approximate dimensions of $4.0 \times 4.0 \times 2.7$ nm^3 (assuming a duplex width of 2 nm and length of ∼0.34 nm per basepair, see Figures 1c,h and S3). To relieve internal strain within this nanostructure, we added 2T or 4T loops (both appear to work equally well, Figure S3) to each of the three duplex crossovers. These 2-strand

https://doi.org/10.1021/acs.nanolett.2c01757
Nano Lett. 2022, 22, 6235−6244

FluoroCubes appeared to emit slightly more photons than full-size 4-strand 1- and 2-dye FluoroCubes, although the two constructs were imaged using different microscopes ($p = 0.033$ and $p = 0.015$, respectively, Figures S3 and S6). These 2-strand FluoroCubes have a similar volume (~45 nm^3) to minimal green fluorescent protein (~36 nm^3),[35] and could potentially be loaded with additional fluorophores via modification of internal sites and the remaining unused strand terminus.

As a control, we performed single molecule photobleaching studies of single Cy3 dyes attached to surface-captured double-stranded DNA (dsDNA; Figure 1h,i). We were able to collect 4× as many photons (1.2 million) per Cy3 dye than reported in the previous work on FluoroCubes[13] (0.3 million). As a result, the 6-dye FluoroCube to 1-dye DNA duplex ratios of photobleaching half-life and total photon count are lower in this work (6.4 ± 0.5× and 12.3 ± 0.6×, respectively) than originally reported[13] (54× and 43×, respectively). (The photobleaching half-life ratio was calculated by multiplying the ratio of k_1 values, 2.9, by 1.13ln(7) − see Supporting Information Note 1). Our ratios are therefore in line with the enhancements reported in the same prior work[13] for dyes other than Cy3. The discrepancy between our work and the previous study may lie in slight differences between buffer conditions, purification strategies, and imaging systems.

$N_{photons}/n$ did not scale significantly with n ($p = 0.069$), suggesting a linear increase in brightness with n. However, this result appeared to be influenced by the high $N_{photons}$ exhibited by 4-dye FluoroCubes (which was indistinguishable from that of 6-dye FluoroCubes, $p = 0.38$). (Increased aggregation was not the source of the high brightness for 4-dye FluoroCubes, Supporting Information Note 2). For $n \neq 4$, $N_{photons}$ scaled sublinearly with n ($p < 0.001$) on-surface (Figure S6), and brightness scaled sublinearly in bulk solution (Figure S7). This suggests that dye−dye interactions such as H-dimerization and singlet−singlet annihilation may actually negatively impact FluoroCube performance by reducing $N_{photons}$.[33,36,37]

To assess the role of dye−dye interactions in FluoroCube performance, we performed statistical comparisons between our single molecule photobleaching measurements. For these comparisons, FluoroCube constructs were grouped according to interdye spacing (for 2-dye Fluorocubes) and n (Figure S8−9, Supporting Information Note 3). While we observed differences in I_0 and $N_{photons}$ as a function of n, these quantities did not differ between 2-dye constructs as a function of interdye spacing. (Few differences in k_1 were observed between constructs). Accordingly, we sought an alternative approach for assessing the role of dye−dye interactions.

Nonfluorescent face-to-face Cy3 H-dimers can be detected via the presence of a large blue-shifted peak[13,32,38] in the Cy3 absorbance spectrum. We measured absorbance spectra of all 14 FluoroCube constructs (Figures 2a,b, S10) and observed H-dimerization in four: 2-dye AB, 3-dye ABC, 5-dye ABC-AC, and 6-dye ABC-ABC. These four constructs (which we call "+H") collectively exhibited significantly fewer $N_{photons}/n$ (photons detected per dye) than the ten other, low H-dimerization constructs (which we call "−H", Figures 2c, S11). None of these constructs were fully quenched, suggesting that H-dimerization is imperfect (i.e., dyes continuously transition between dimeric and monomeric states).[37] The +H and -H groups showed no significant difference in k_1 (Figures 2d, S11), suggesting that H-dimerization does not alter photobleaching kinetics.

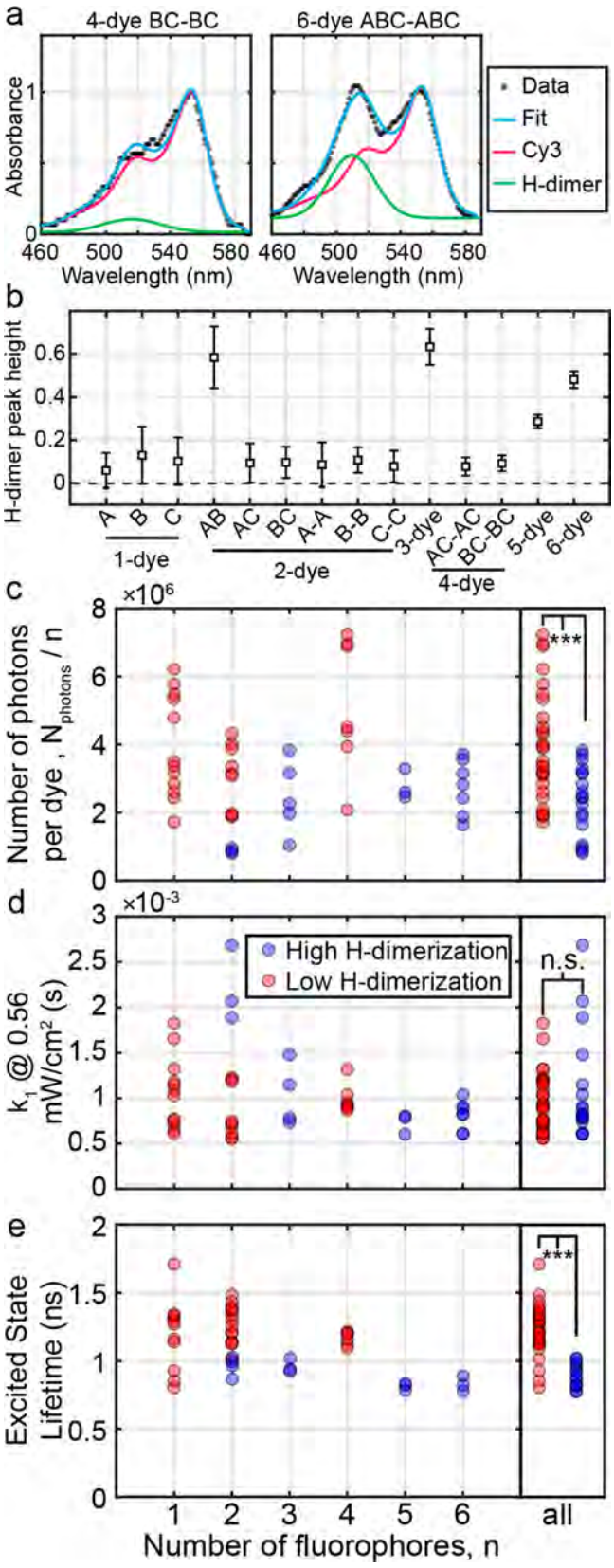

Figure 2. H-dimerization can perturb FluoroCube function. (a) Representative absorbance spectra of 4-dye BC-BC (left) and 6-dye ABC-ABC FluoroCubes. A curve fit, consisting of a Cy3 spectrum plus an H-dimer peak centered on ~515 nm (see Figure S10 for more information) is shown in cyan. The two components of the curve fit are shown in magenta and green. (b) The height of the H-dimer component of the absorbance spectrum fit (best fit ± 95% confidence

https://doi.org/10.1021/acs.nanolett.2c01757
Nano Lett. 2022, 22, 6235−6244

Figure 2. continued

interval of the fit), normalized to the height of the Cy3 spectrum component, is shown for each of the 14 constructs studied in this work. Four constructs (2-dye AB, 3-dye ABC, 5-dye ABC-AC, and 6-dye ABC-ABC) stand out as exhibiting heightened levels of H-dimerization. (c–e) Scattered points showing individual measurements $N_{photons}/n$ (b), k_1 (c), and the excited state fluorescence lifetime (d) measured as a function of n. Red and blue scatter points show FluoroCubes that exhibit low and high degrees of H-dimerization, respectively. Two-sided t tests comparing all constructs in high and low H-dimerization groups (right side of each plot) showed that the constructs with high degrees of H-dimerization emit fewer total photons and have shorter excited state lifetimes than their low H-dimerization counterparts yet exhibit the same rate of photobleaching (*** denotes $p < 0.001$, n.s. denotes $p > 0.05$).

The intensity of single +H FluoroCubes fluctuated significantly more than −H FluoroCubes (Figure S12). We ascribe this observation to the increased number of discrete brightness levels that are possible when dyes can exist in (and transition between) monomeric and dimeric states. The 4-dye FluoroCubes exhibited the fewest intensity fluctuations of all constructs. Altogether, reducing n from six to four significantly reduces intensity fluctuations without compromising total photon count, brightness, or photostability—thus representing an overall improvement in performance at reduced cost.

We noticed that H-dimerization only occurred in constructs with a pair (or two pairs) of dyes that were 1) on adjacent duplexes, and 2) both attached to a terminal A-T pair. Cyanine dyes are known to stack against the termini of the DNA duplexes they are coupled to, and the energy of stacking to a terminal G-C is ∼2–4 kcal/mol higher than stacking to a terminal A-T.[39] Therefore, it appears that H-dimerization may only occur when two fluorophores are close (within ∼2 nm) and are both unstacked from their respective DNA duplex termini. Perhaps in future work, FluoroCube performance can be improved by strategically mutating terminal basepairs to limit H-dimerization.

We also measured the excited-state fluorescence lifetimes (Figures 2e, S13, and S14) and time-resolved fluorescence anisotropies (Figure S13b) of our 14 constructs. The fluorescence lifetime was significantly shorter for +H constructs than -H constructs ($p < 0.001$), and correlated negatively with n for +H constructs ($p < 0.01$) but not -H constructs ($p = 0.74$). Decreased excited state lifetime is a hallmark of fluorescence quenching and H-dimerization due to increased competition between radiative and nonradiative energy decay pathways. Fluorescence anisotropy negatively correlated with n, which we attribute to FRET between Cy3 dyes (homoFRET, Figures S15 and S16). While homoFRET alone is not expected to reduce FluoroCube brightness, its presence suggests that singlet–singlet annihilation (which

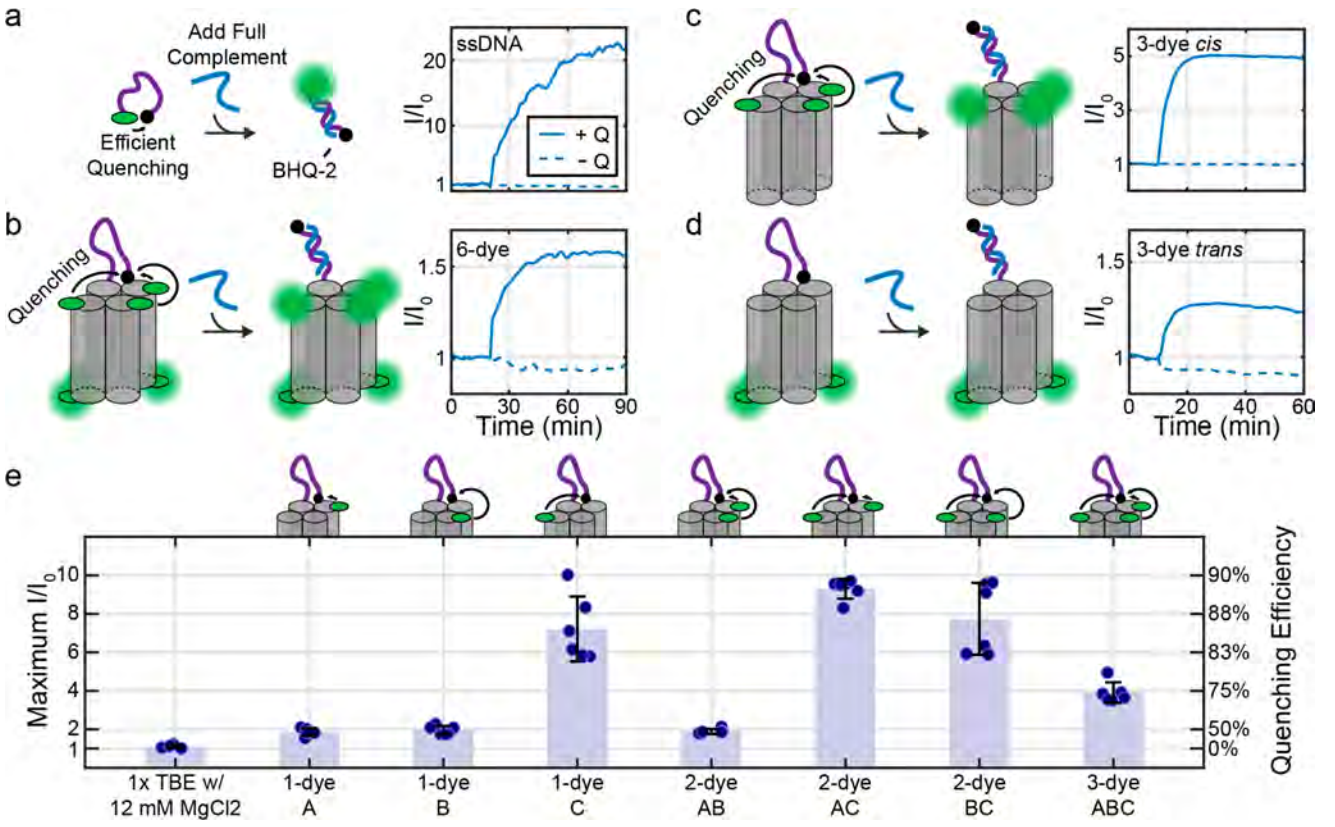

Figure 3. FluoroCubes are compatible with dark quenching applications. (a) Schematic of single-stranded 15 nt fluorogenic DNA exhibiting dequenching upon hybridization to a full complement (left) and in-solution normalized fluorescence intensity before and after equimolar addition of a full complement oligonucleotide in 4× PBS (right). (b–d) Same as panel a, but for 6-dye, 3-dye cis, and 3-dye trans FluoroCubes in 1× TBE with 12 mM $MgCl_2$. Note that all four plots in a–d have different y-axis scales and have dashed curves showing the results of control experiments performed in the absence of BHQ-2 quenchers. (e) Maximum in-solution normalized fluorescence intensity from seven 1-, 2-, and 3-dye cis FluoroCube constructs, as well as a FluoroCube-free control. Circles show individual data points from six experimental replicates, whereas bars and errorbars show average and standard deviation of replicates. The right y-axis shows the quenching efficiency at each grid line.

https://doi.org/10.1021/acs.nanolett.2c01757
Nano Lett. 2022, 22, 6235–6244

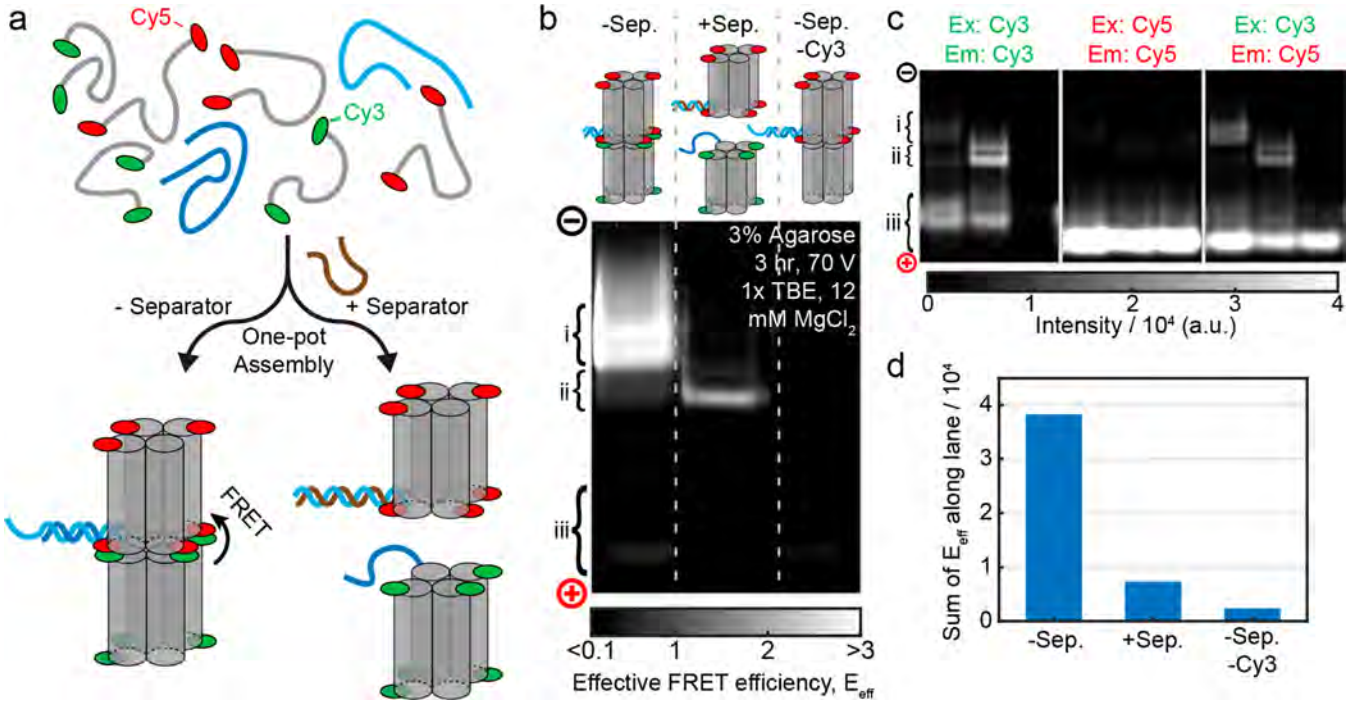

Figure 4. FluoroCubes are compatible with FRET applications. (a) Schematic depiction of the one-pot assembly of Cy3-Cy5 FluoroCube complexes from eight strands (left) or separated FluoroCubes with the addition of a separator strand. (b) Image of the effective FRET efficiency E_{eff} of single and complexed FluoroCubes in a 3% agarose gel after 3 h of gel electrophoresis. (c) The raw images used to calculate E_{eff} (the lanes are the same as in (b). Gel images are labeled on the left with a + and − end showing that the electrophoretic direction was from top (−) to bottom (+) in the image. Curly brackets show the approximate coordinates that were generally interpreted as containing assembled FluoroCube complexes (i), individual FluoroCubes (ii), or incomplete FluoroCubes and unassembled single strands (iii). We expect that the presence of multiple bands in ii and iii is the result of end-to-end stacking between FluoroCubes. (d) Integrated E_{eff} for the three lanes (this is mathematically valid because E_{eff} is proportional to the concentration of FRET complex) showing very high FRET for only the complexed FluoroCubes with both Cy3 and Cy5 dyes.

reduces brightness at high laser power via a similar process to homoFRET) may occur. Consistent with this expectation (and with prior work[13]), brightness/n was negatively correlated with n at high laser powers (Figure S15). See Supporting Information Note 4 for additional discussion of homoFRET and annihilation.

We next tested the compatibility of FluoroCubes with dark quenchers. Previous work has shown that unstructured DNA oligonucleotides (~15 nt in length) flanked by fluorophore-quencher pairs exhibit high fluorogenicity (i.e., their brightness strongly increases upon hybridization to a complementary oligonucleotide, Figure 3a).[22,23] To apply this principle to FluoroCubes, we appended a 15 nt single-stranded overhang with a terminal black hole quencher (BHQ-2) to a 6-dye FluoroCube (Figure 3b), expecting that the BHQ-2 would form a ground-state complex with (and thus quench) the Cy3 dyes on the same face as the overhang (Figure 3a). To assess quenching efficiency, we measured in-solution fluorescence intensity before and after the addition of a complement strand, which hybridizes to the overhang and thus separates the quencher from the Cy3 dyes.[22,23]

The 6-dye fluorogenic FluoroCube's fluorescence increased by ~60% following hybridization, (Figure 3b). For reference, the overhang strand alone flanked by Cy5 and BHQ-2 exhibited a ~20×, or 2,000%, increase (Figure 3a). We hypothesized that the lower fluorogenicity of the 6-dye FluoroCube could be explained by moderate quenching of the three fluorophores on the same face as the overhang and inefficient quenching of the three fluorophores on the opposite face. To test this hypothesis, we designed two 3-dye FluoroCubes: one with three fluorophores on the same side as the quencher overhang (cis, Figures 3c and S17b), and one with three fluorophores on the opposite side (*trans*, Figure 3d and S17b). The 3-dye cis- and trans-FluoroCubes exhibited 400% and 25% increase in fluorescence upon hybridization, respectively (Figure 3c,d). The 400% increase for the 3-dye cis FluoroCube corresponds to an 80% quenching efficiency.

To determine whether the quenching efficiency could be increased beyond 80%, we assembled and tested six additional *cis* FluoroCube constructs (Figure S17). Specifically, we designed three 1-dye cis Fluorocube constructs, each with a fluorophore in one of three positions (denoted A, B, and C as shown in Figure 3e) and three 2-dye *cis* Fluorocube constructs, each with two fluorophores in a unique combination of those positions. The 1-dye A, 1-dye B, and 2-dye AB constructs all exhibited a ~ 50% quenching efficiency, which was significantly lower than that of the 3-dye cis-FluoroCube ($p < 0.01$, Figure 3e). However, the 1-dye C, 2-dye AC, and 2-dye BC constructs each exhibited enhanced (85−90%) quenching efficiencies, which were significantly higher than that of the 3-dye cis-FluoroCube construct ($p < 0.01$, Figure 3e).

To summarize, quenching efficiency appears to be maximized when a fluorophore is in position C and there are either no additional fluorophores or one fluorophore in either position A or position B (but not both). The site dependence of fluorogenicity is likely the result of localized properties such as linkage strategy, DNA sequence, and H-dimerization,[13,40] Such local properties, as well as localized properties of neighboring dyes, likely affect the extent to which the quencher can interact with the dye. As pointed out in the section on H-

https://doi.org/10.1021/acs.nanolett.2c01757
Nano Lett. 2022, 22, 6235−6244

dimerization, the dye in the C-position is flanked immediately by a C-G pair, while the A- and B-position dyes are flanked by A-T pairs (Table S1). Accordingly, the C-position dye could be expected to spend more time directly stacked against its duplex's terminus.[39] Conversely, the A- and B-position dyes are bound to less thermodynamically stable duplex termini, and thus may spend more time in an unstacked state due to duplex "breathing".[41] Perhaps the DNA-stacked fluorophore at the C-position is more readily available for contact quenching by BHQ-2 than the unstacked fluorophores at the A- and B-positions and, following recruitment to the C-position, the quencher can efficiently quench one additional unstacked fluorophore.

Finally, we examined whether FluoroCubes could be used in FRET applications. Via one-pot assembly, we coassembled a 6-dye Cy3 FluoroCube (donor) and a 6-dye Cy5 FluoroCube (acceptor) attached via complementary single-stranded DNA overhangs (Figure 4a). We also performed the same assembly in the presence of excess "separator" strand, which binds to the Cy5 FluoroCube's overhang more stably (21 bp) than the Cy3 FluoroCube's overhang does (15 bp). (The separator can also displace the Cy3 FluoroCube's overhang through toehold-mediated strand displacement.) We then performed agarose gel electrophoresis for 3 h postassembly and imaged the gel to measure the effective FRET efficiency (E_{eff}, an imperfect quantifier of FRET that is proportional to the concentration of donor−acceptor complex, Figures 4b,c, and S18). In the absence of the separator, a low mobility band (assembled complex) exhibited high E_{eff} (Figure 4b−d). In the presence of the separator strand, the low mobility band disappeared and was replaced by higher mobility bands (individual FluoroCubes), which exhibited low E_{eff} (Figure 4b−d). When the separator and all six dyes on the Cy3 FluoroCube were removed, the low mobility band was recovered, but the E_{eff} of this band remained low (Figure 4b-d). Similar results were observed when using a 3-dye *cis* Cy3 FluoroCube, and with 3- and 6-dye Cy3 fluorogenic FluoroCubes (Figure S19). These results demonstrate that FluoroCubes are compatible with FRET applications.

The current work presents evidence that Cy3 FluoroCube ultraphotostability arises from dye−DNA interactions, rather than dye−dye interactions. We expect that the same is true for FluoroCubes with other dyes, particularly structural analogs like Cy5. Cy3 is known to photobleach through two parallel pathways: isomerization and photo-oxidation.[42] The four-helix bundle may inhibit isomerization by interacting through stacking interactions[43] with the Cy3 and stabilizing the bright isomer.[7,27] The bundle may also inhibit photo-oxidation by excluding oxygen from the fluorophores' local environment or by altering the electronic structure of the dye's excited state[7] (as indicated by changes to Cy3 FluoroCubes' emission spectra[13]). Similar levels of photostabilization have been observed when Cy3 is attached internally to double stranded DNA[27] (and even proteins[44,45]), suggesting that the presence of multiple bundled DNA duplex termini further compound such effects. For future work, this interpretation naturally raises important questions: How much further can photostability be enhanced by attaching dyes to larger DNA bundles or labeling them internally, deep within dense DNA origami nanostructures? Do bundled DNA nanostructures generally confer stabilization to certain fluorophores? Recent work has shown that fluorophores can interact with DNA nanotechnology through a variety of interactions modes (e.g., base stacking, groove binding, binding to crossovers) that are highly sensitive to attachment chemistry and local DNA environment.[46] Some of these interactions are unique to multihelix structural motifs. We find it likely that single molecule photobleaching studies of existing DNA-based technologies[47,48] may reveal photostability that exceeds what has already been shown.

Dye−dye interactions, on the other hand, appear to undermine FluoroCube quality.[37] Our work suggests that 4-dye FluoroCubes may be optimal, potentially because they best balance the trade-off between having increased brightness due to increased n and an increase in self-quenching interactions due to crowding of fluorophores into a small space. Four-dye FluoroCubes also benefit from having two additional free DNA termini that can be labeled with useful chemical tags such as triplet state quenchers,[49] photoprotective agents,[50] and targeting motifs.[51] Even four-dye FluoroCubes will likely suffer from brightness reduction at very high laser powers due to singlet−singlet annihilation. However, the control and programmability offered by DNA nanotechnology suggests that similar processes with desirable outcomes—such as triplet−triplet annihilation for photon upconversion—could be rationally engineered using FluoroCube-like technologies.[52]

This work also demonstrates that FluoroCubes are compatible with FRET and dark quenching applications. Extension of these principles to single molecule applications could enable high signal-to-noise studies of molecular conformational dynamics with unprecedented duration (>1 h).[15,53] The high photostability of individual FluoroCubes, even in the absence of OSS (FluoroCubes without OSS have comparable photostability to individual fluorophores in OSS[13]) could allow such studies, typically performed on purified biochemicals conjugated to glass, to be performed within living cells and other more complex systems. The similarity in size between FluoroCubes (particularly miniature 2-strand FluoroCubes) and genetically encoded fluorescent proteins speaks to the feasibility of such techniques. Cytosolic delivery of FluoroCubes is a challenge that may necessitate microinjection or plasma membrane permeabilization.[54] Susceptibility to nuclease degradation is also a potential concern, although it is also possible that, similar to other DNA nanostructures, FluoroCubes exhibit increased resistance to nucleases.[55]

The tight packing of dyes on a FluoroCube enables simultaneous quenching of multiple fluorophores by a single dark quencher (Figure 2). The maximum quenching efficiency of ~90% can potentially be improved further with the use of multiple quenchers[56] and/or sequence refinement. Fluorogenic FluoroCubes are likely compatible with existing techniques such as molecular tension fluorescence microscopy[24,25,57−60] and fluorogenic DNA PAINT.[22] Because dark quenchers are known to shield fluorophores from photobleaching,[61] fluorogenic FluoroCubes may one day enable DNA PAINT[22,60,62] and kinetic fingerprinting-type[19,63,64] applications in which the imagers are under constant illumination, confined to fixed compartments (e.g., live cells) without the ability to exchange with the surrounding environment.

■ ASSOCIATED CONTENT

Supporting Information

The Supporting Information is available free of charge at https://pubs.acs.org/doi/10.1021/acs.nanolett.2c01757.

https://doi.org/10.1021/acs.nanolett.2c01757
Nano Lett. 2022, 22, 6235−6244

Experimental and computational methods, supplemental Figures S1−S19, supplemental Tables 1−2, and supplemental Notes 1−4 (PDF)

AUTHOR INFORMATION

Corresponding Author

Nils G. Walter − *Single Molecule Analysis Group, Department of Chemistry and Center for RNA Biomedicine, University of Michigan, Ann Arbor, Michigan 48109, United States;* orcid.org/0000-0002-7301-1275; Email: nwalter@umich.edu

Authors

Aaron T. Blanchard − *Single Molecule Analysis Group, Department of Chemistry, Department of Biomedical Engineering, and Michigan Society of Fellows, University of Michigan, Ann Arbor, Michigan 48109, United States;* Present Address: Department of Biomedical Engineering, Duke University, Durham, North Carolina, 27705, United States; orcid.org/0000-0002-3129-6591

Zi Li − *Single Molecule Analysis Group, Department of Chemistry, University of Michigan, Ann Arbor, Michigan 48109, United States;* Present Address: Pacific Biosciences, Menlo Park, California, 94025, United States.

Elizabeth C. Duran − *Single Molecule Analysis Group, Department of Chemistry, University of Michigan, Ann Arbor, Michigan 48109, United States*

Catherine E. Scull − *Single Molecule Analysis Group, Department of Chemistry, University of Michigan, Ann Arbor, Michigan 48109, United States*

J. Damon Hoff − *Single Molecule Analysis in Real-Time (SMART) Center, University of Michigan, Ann Arbor, Michigan 48109, United States*

Keenan R. Wright − *Department of Chemistry, University of Michigan, Ann Arbor, Michigan 48109, United States*

Victor Pan − *Department of Biomedical Engineering, Emory University and the Georgia Institute of Technology, Atlanta, Georgia 30322;* Present Address: Intellia Therapeutics, Cambridge, Massachusetts 02139, United States.

Complete contact information is available at: https://pubs.acs.org/10.1021/acs.nanolett.2c01757

Author Contributions

All authors have given approval to the final version of the manuscript.

Notes

The authors declare no competing financial interest.

ACKNOWLEDGMENTS

We acknowledge use of the Single Particle Tracker equipment in the Single Molecule Analysis in Real-Time (SMART) Center at the University of Michigan, seeded by NSF MRI-ID grant DBI-0959823. We thank Viktorjia Glembockyte and Philip Tinnefeld (LMU Munich) for helpful conversations. This work was supported by the United States National Institutes of Health (NIH) in the form of Grants R35 GM131922, R21 CA204560, and R33 CA229023 to N.G.W., F32 GM140547 to C.E.S., NIH IRACDA fellowship Grant K12 GM111725 to E.C.D., and K00 CA245789 to A.T.B..

ABBREVIATIONS

DNA, deoxyribonucleic acid; FRET, Förster resonance energy transfer; SA, streptavidin; Cy3, cyanine 3; Cy5, cyanine 5; BHQ-2, black hole quencher 2; OSS, oxygen scavenging system; PAINT, points accumulation for imaging in nanoscale topology; PEG, poly(ethylene glycol); PCA, protocatechuic acid; PCD, protocatechuate-3,4-dioxygenase

REFERENCES

(1) Zheng, Q.; Juette, M. F.; Jockusch, S.; Wasserman, M. R.; Zhou, Z.; Altman, R. B.; Blanchard, S. C. Ultra-stable organic fluorophores for single-molecule research. *Chem. Soc. Rev.* **2014**, *43* (4), 1044−1056.

(2) Renikuntla, B. R.; Rose, H. C.; Eldo, J.; Waggoner, A. S.; Armitage, B. A. Improved Photostability and Fluorescence Properties through Polyfluorination of a Cyanine Dye. *Org. Lett.* **2004**, *6* (6), 909−912.

(3) Toutchkine, A.; Nguyen, D.-V.; Hahn, K. M. Merocyanine Dyes with Improved Photostability. *Org. Lett.* **2007**, *9* (15), 2775−2777.

(4) Aitken, C. E.; Marshall, R. A.; Puglisi, J. D. An Oxygen Scavenging System for Improvement of Dye Stability in Single-Molecule Fluorescence Experiments. *Biophys. J.* **2008**, *94* (5), 1826−1835.

(5) Rasnik, I.; McKinney, S. A.; Ha, T. Nonblinking and long-lasting single-molecule fluorescence imaging. *Nat. Methods* **2006**, *3* (11), 891−893.

(6) Glembockyte, V.; Lincoln, R.; Cosa, G. Cy3 Photoprotection Mediated by Ni2+ for Extended Single-Molecule Imaging: Old Tricks for New Techniques. *J. Am. Chem. Soc.* **2015**, *137* (3), 1116−1122.

(7) Glembockyte, V.; Frenette, M.; Mottillo, C.; Durantini, A. M.; Gostick, J.; Štrukil, V.; Friščić, T.; Cosa, G. Highly Photostable and Fluorescent Microporous Solids Prepared via Solid-State Entrapment of Boron Dipyrromethene Dyes in a Nascent Metal−Organic Framework. *J. Am. Chem. Soc.* **2018**, *140* (49), 16882−16887.

(8) Guether, R.; Reddington, M. V. Photostable Cyanine Dye β-Cyclodextrin Conjugates. *Tetrahedron Lett.* **1997**, *38* (35), 6167−6170.

(9) Yau, C. M. S.; Pascu, S. I.; Odom, S. A.; Warren, J. E.; Klotz, E. J. F.; Frampton, M. J.; Williams, C. C.; Coropceanu, V.; Kuimova, M. K.; Phillips, D.; Barlow, S.; Brédas, J.-L.; Marder, S. R.; Millar, V.; Anderson, H. L. Stabilisation of a heptamethine cyanine dye by rotaxane encapsulation. *Chem. Commun.* **2008**, No. 25, 2897−2899.

(10) Yang, S. K.; Shi, X.; Park, S.; Ha, T.; Zimmerman, S. C. A dendritic single-molecule fluorescent probe that is monovalent, photostable and minimally blinking. *Nat. Chem.* **2013**, *5* (8), 692−697.

(11) Mohanty, J.; Nau, W. M. Ultrastable Rhodamine with Cucurbituril. *Angew. Chem., Int. Ed.* **2005**, *44* (24), 3750−3754.

(12) Chen, M.; Yin, M. Design and development of fluorescent nanostructures for bioimaging. *Prog. Polym. Sci.* **2014**, *39* (2), 365−395.

(13) Niekamp, S.; Stuurman, N.; Vale, R. D. A 6-nm ultra-photostable DNA FluoroCube for fluorescence imaging. *Nat. Methods* **2020**, *17* (4), 437−441.

(14) Niekamp, S.; Stuurman, N.; Zhang, N.; Vale, R. D. Three-color single-molecule imaging reveals conformational dynamics of dynein undergoing motility. *Proc. Natl. Acad. Sci. U. S. A.* **2021**, *118* (31), e2101391118.

(15) Sasmal, D. K.; Pulido, L. E.; Kasal, S.; Huang, J. Single-molecule fluorescence resonance energy transfer in molecular biology. *Nanoscale* **2016**, *8* (48), 19928−19944.

(16) Pehlivan, Z. S.; Torabfam, M.; Kurt, H.; Ow-Yang, C.; Hildebrandt, N.; Yüce, M. Aptamer and nanomaterial based FRET biosensors: a review on recent advances (2014−2019). *Microchimica Acta* **2019**, *186* (8), 563.

(17) Rowland, C. E.; Brown, C. W.; Medintz, I. L.; Delehanty, J. B. Intracellular FRET-based probes: a review. *Methods and applications in fluorescence* **2015**, *3* (4), 042006.

(18) Ham, T. R.; Collins, K. L.; Hoffman, B. D. Molecular tension sensors: moving beyond force. *Current Opinion in Biomedical Engineering* **2019**, *12*, 83−94.
(19) Khanna, K.; Mandal, S.; Blanchard, A. T.; Tewari, M.; Johnson-Buck, A.; Walter, N. G. Rapid kinetic fingerprinting of single nucleic acid molecules by a FRET-based dynamic nanosensor. *Biosens. Bioelectron.* **2021**, *190*, 113433.
(20) Ryazantsev, D. Y.; Kvach, M. V.; Tsybulsky, D. A.; Prokhorenko, I. A.; Stepanova, I. A.; Martynenko, Y. V.; Gontarev, S. V.; Shmanai, V. V.; Zavriev, S. K.; Korshun, V. A. Design of molecular beacons: 3′ couple quenchers improve fluorogenic properties of a probe in real-time PCR assay. *Analyst* **2014**, *139* (11), 2867−2872.
(21) Zheng, J.; Yang, R.; Shi, M.; Wu, C.; Fang, X.; Li, Y.; Li, J.; Tan, W. Rationally designed molecular beacons for bioanalytical and biomedical applications. *Chem. Soc. Rev.* **2015**, *44* (10), 3036−3055.
(22) Chung, K. K. H.; Zhang, Z.; Kidd, P.; Zhang, Y.; Williams, N. D.; Rollins, B.; Yang, Y.; Lin, C.; Baddeley, D.; Bewersdorf, J. Fluorogenic probe for fast 3D whole-cell DNA-PAINT. *bioRxiv* 2020, 2020.04.29.066886.
(23) Kashida, H.; Morimoto, K.; Asanuma, H. A stem-less probe using spontaneous pairing between Cy3 and quencher for RNA detection. *Sci. Technol. Adv. Mater.* **2016**, *17* (1), 267−273.
(24) Zhang, Y.; Ge, C.; Zhu, C.; Salaita, K. DNA-based digital tension probes reveal integrin forces during early cell adhesion. *Nat. Commun.* **2014**, *5*, 5167.
(25) Brockman, J. M.; Blanchard, A. T.; Pui-Yan Ma, V.; Derricotte, W. D.; Zhang, Y.; Fay, M. E.; Lam, W. A.; Evangelista, F. A.; Mattheyses, A. L.; Salaita, K. Mapping the 3D orientation of piconewton integrin traction forces. *Nat. Methods* **2018**, *15*, 115.
(26) Marras, S. A. E. Efficiencies of fluorescence resonance energy transfer and contact-mediated quenching in oligonucleotide probes. *Nucleic Acids Res.* **2002**, *30* (21), 122e.
(27) Lee, W.; von Hippel, P. H.; Marcus, A. H. Internally labeled Cy3/Cy5 DNA constructs show greatly enhanced photo-stability in single-molecule FRET experiments. *Nucleic Acids Res.* **2014**, *42* (9), 5967−5977.
(28) Pace, N. A.; Hennelly, S. P.; Goodwin, P. M. Immobilization of Cyanines in DNA Produces Systematic Increases in Fluorescence Intensity. *J. Phys. Chem. Lett.* **2021**, *12* (37), 8963−8971.
(29) Sorour, M. I.; Kistler, K. A.; Marcus, A. H.; Matsika, S. Accurate Modeling of Excitonic Coupling in Cyanine Dye Cy3. *J. Phys. Chem. A* **2021**, *125* (36), 7852−7866.
(30) Banal, J. L.; Kondo, T.; Veneziano, R.; Bathe, M.; Schlau-Cohen, G. S. Photophysics of J-Aggregate-Mediated Energy Transfer on DNA. *J. Phys. Chem. Lett.* **2017**, *8* (23), 5827−5833.
(31) Kringle, L.; Sawaya, N. P. D.; Widom, J.; Adams, C.; Raymer, M. G.; Aspuru-Guzik, A.; Marcus, A. H. Temperature-dependent conformations of exciton-coupled Cy3 dimers in double-stranded DNA. *J. Chem. Phys.* **2018**, *148* (8), 085101.
(32) Huff, J. S.; Davis, P. H.; Christy, A.; Kellis, D. L.; Kandadai, N.; Toa, Z. S. D.; Scholes, G. D.; Yurke, B.; Knowlton, W. B.; Pensack, R. D. DNA-Templated Aggregates of Strongly Coupled Cyanine Dyes: Nonradiative Decay Governs Exciton Lifetimes. *J. Phys. Chem. Lett.* **2019**, *10* (10), 2386−2392.
(33) Helmerich, D. A.; Beliu, G.; Sauer, M. Multiple-Labeled Antibodies Behave Like Single Emitters in Photoswitching Buffer. *ACS Nano* **2020**, *14* (10), 12629−12641.
(34) Saurabh, A.; Niekamp, S.; Sgouralis, I.; Pressé, S. Modeling Non-additive Effects in Neighboring Chemically Identical Fluorophores. *arXiv e-prints* 2022, arXiv:2202.07039.
(35) Yang, F.; Moss, L. G.; Phillips, G. N. The molecular structure of green fluorescent protein. *Nat. Biotechnol.* **1996**, *14* (10), 1246−1251.
(36) Hofkens, J.; Cotlet, M.; Vosch, T.; Tinnefeld, P.; Weston, K. D.; Ego, C.; Grimsdale, A.; Müllen, K.; Beljonne, D.; Brédas, J. L.; Jordens, S.; Schweitzer, G.; Sauer, M.; De Schryver, F. Revealing competitive Förster-type resonance energy-transfer pathways in single bichromophoric molecules. *Proc. Natl. Acad. Sci. U. S. A.* **2003**, *100* (23), 13146.
(37) Schröder, T.; Scheible, M. B.; Steiner, F.; Vogelsang, J.; Tinnefeld, P. Interchromophoric Interactions Determine the Maximum Brightness Density in DNA Origami Structures. *Nano Lett.* **2019**, *19* (2), 1275−1281.
(38) Nicoli, F.; Roos, M. K.; Hemmig, E. A.; Di Antonio, M.; de Vivie-Riedle, R.; Liedl, T. Proximity-Induced H-Aggregation of Cyanine Dyes on DNA-Duplexes. *J. Phys. Chem. A* **2016**, *120* (50), 9941−9947.
(39) Spiriti, J.; Binder, J. K.; Levitus, M.; van der Vaart, A. Cy3-DNA stacking interactions strongly depend on the identity of the terminal basepair. *Biophys. J.* **2011**, *100* (4), 1049−1057.
(40) Kretschy, N.; Sack, M.; Somoza, M. M. Sequence-Dependent Fluorescence of Cy3- and Cy5-Labeled Double-Stranded DNA. *Bioconjugate Chem.* **2016**, *27* (3), 840−848.
(41) Jose, D.; Datta, K.; Johnson, N. P.; von Hippel, P. H. Spectroscopic studies of position-specific DNA "breathing" fluctuations at replication forks and primer-template junctions. *Proc. Natl. Acad. Sci. U. S. A.* **2009**, *106* (11), 4231.
(42) Jouonang, A. L.; Didier, P.; Mély, Y. Identification of a thermally activated process in the Cy3 photobleaching mechanism. *Phys. Chem. Chem. Phys.* **2012**, *14* (5), 1585−1588.
(43) Iqbal, A.; Arslan, S.; Okumus, B.; Wilson, T. J.; Giraud, G.; Norman, D. G.; Ha, T.; Lilley, D. M. J. Orientation dependence in fluorescent energy transfer between Cy3 and Cy5 terminally attached to double-stranded nucleic acids. *Proc. Natl. Acad. Sci. U. S. A.* **2008**, *105* (32), 11176.
(44) Rashid, F.; Raducanu, V.-S.; Zaher, M. S.; Tehseen, M.; Habuchi, S.; Hamdan, S. M. Initial state of DNA-Dye complex sets the stage for protein induced fluorescence modulation. *Nat. Commun.* **2019**, *10* (1), 2104.
(45) Lerner, E.; Ploetz, E.; Hohlbein, J.; Cordes, T.; Weiss, S. A Quantitative Theoretical Framework For Protein-Induced Fluorescence Enhancement−Förster-Type Resonance Energy Transfer (PIFE-FRET). *J. Phys. Chem. B* **2016**, *120* (26), 6401−6410.
(46) Hübner, K.; Joshi, H.; Aksimentiev, A.; Stefani, F. D.; Tinnefeld, P.; Acuna, G. P. Determining the In-Plane Orientation and Binding Mode of Single Fluorescent Dyes in DNA Origami Structures. *ACS Nano* **2021**, *15* (3), 5109−5117.
(47) Woehrstein, J. B.; Strauss, M. T.; Ong, L. L.; Wei, B.; Zhang, D. Y.; Jungmann, R.; Yin, P. Sub−100-nm metafluorophores with digitally tunable optical properties self-assembled from DNA. *Sci. Adv.* **2017**, *3* (6), e1602128.
(48) Pan, V.; Wang, W.; Heaven, I.; Bai, T.; Cheng, Y.; Chen, C.; Ke, Y.; Wei, B. Monochromatic Fluorescent Barcodes Hierarchically Assembled from Modular DNA Origami Nanorods. *ACS Nano* **2021**, *15*, 15892.
(49) Altman, R. B.; Terry, D. S.; Zhou, Z.; Zheng, Q.; Geggier, P.; Kolster, R. A.; Zhao, Y.; Javitch, J. A.; Warren, J. D.; Blanchard, S. C. Cyanine fluorophore derivatives with enhanced photostability. *Nat. Methods* **2012**, *9* (1), 68−71.
(50) Zheng, Q.; Jockusch, S.; Zhou, Z.; Altman, R. B.; Zhao, H.; Asher, W.; Holsey, M.; Mathiasen, S.; Geggier, P.; Javitch, J. A.; Blanchard, S. C. Electronic tuning of self-healing fluorophores for live-cell and single-molecule imaging. *Chemical Science* **2017**, *8* (1), 755−762.
(51) Lee, H.; Lytton-Jean, A. K. R.; Chen, Y.; Love, K. T.; Park, A. I.; Karagiannis, E. D.; Sehgal, A.; Querbes, W.; Zurenko, C. S.; Jayaraman, M.; Peng, C. G.; Charisse, K.; Borodovsky, A.; Manoharan, M.; Donahoe, J. S.; Truelove, J.; Nahrendorf, M.; Langer, R.; Anderson, D. G. Molecularly self-assembled nucleic acid nanoparticles for targeted in vivo siRNA delivery. *Nat. Nanotechnol.* **2012**, *7* (6), 389−393.
(52) Ahmad, W.; Wang, J.; Li, H.; Ouyang, Q.; Wu, W.; Chen, Q. Strategies for combining triplet−triplet annihilation upconversion sensitizers and acceptors in a host matrix. *Coord. Chem. Rev.* **2021**, *439*, 213944.
(53) Le Reste, L.; Hohlbein, J.; Gryte, K.; Kapanidis, A. N. Characterization of dark quencher chromophores as nonfluorescent

https://doi.org/10.1021/acs.nanolett.2c01757
Nano Lett. 2022, 22, 6235−6244

acceptors for single-molecule FRET. *Biophys. J.* **2012**, *102* (11), 2658−2668.
(54) Balakrishnan, D.; Wilkens, G. D.; Heddle, J. G. Delivering DNA origami to cells. *Nanomedicine* **2019**, *14* (7), 911−925.
(55) Chandrasekaran, A. R. Nuclease resistance of DNA nanostructures. *Nature Reviews Chemistry* **2021**, *5* (4), 225−239.
(56) Hirotsu, Y.; Mochizuki, H.; Omata, M. Double-quencher probes improve detection sensitivity toward Severe Acute Respiratory Syndrome Coronavirus 2 (SARS-CoV-2) in a reverse-transcription polymerase chain reaction (RT-PCR) assay. *J. Virol. Methods* **2020**, *284*, 113926−113926.
(57) Dutta, P. K.; Zhang, Y.; Blanchard, A. T.; Ge, C.; Rushdi, M.; Weiss, K.; Zhu, C.; Ke, Y.; Salaita, K. Programmable Multivalent DNA-Origami Tension Probes for Reporting Cellular Traction Forces. *Nano Lett.* **2018**, *18* (8), 4803−4811.
(58) Zhang, Y.; Qiu, Y.; Blanchard, A. T.; Chang, Y.; Brockman, J. M.; Ma, V. P.-Y.; Lam, W. A.; Salaita, K. Platelet integrins exhibit anisotropic mechanosensing and harness piconewton forces to mediate platelet aggregation. *Proc. Natl. Acad. Sci. U. S. A.* **2018**, *115* (2), 325.
(59) Blanchard, A. T.; Salaita, K. Emerging uses of DNA mechanical devices. *Science* **2019**, *365* (6458), 1080−1081.
(60) Brockman, J. M.; Su, H.; Blanchard, A. T.; Duan, Y.; Meyer, T.; Quach, M. E.; Glazier, R.; Bazrafshan, A.; Bender, R. L.; Kellner, A. V.; Ogasawara, H.; Ma, R.; Schueder, F.; Peitrich, B. G.; Jungmann, R.; Li, R.; Mattheyses, A. L.; Ke, Y.; Salaita, K. Live-cell super-resolved PAINT imaging of pN cellular traction forces. *Nat. Methods* **2020**, *17* (10), 1018−1024.
(61) Ma, R.; Kellner, A. V.; Ma, V. P.-Y.; Su, H.; Deal, B. R.; Brockman, J. M.; Salaita, K. DNA probes that store mechanical information reveal transient piconewton forces applied by T cells. *Proc. Natl. Acad. Sci. U. S. A.* **2019**, *116* (34), 16949.
(62) Jungmann, R.; Avendaño, M. S.; Woehrstein, J. B.; Dai, M.; Shih, W. M.; Yin, P. Multiplexed 3D cellular super-resolution imaging with DNA-PAINT and Exchange-PAINT. *Nat. Methods* **2014**, *11* (3), 313−318.
(63) Johnson-Buck, A.; Su, X.; Giraldez, M. D.; Zhao, M.; Tewari, M.; Walter, N. G. Kinetic fingerprinting to identify and count single nucleic acids. *Nat. Biotechnol.* **2015**, *33* (7), 730−732.
(64) Chatterjee, T.; Knappik, A.; Sandford, E.; Tewari, M.; Choi, S. W.; Strong, W. B.; Thrush, E. P.; Oh, K. J.; Liu, N.; Walter, N. G.; Johnson-Buck, A. Direct kinetic fingerprinting and digital counting of single protein molecules. *Proc. Natl. Acad. Sci. U.S.A.* **2020**, *117* (37), 22815−22822.

https://doi.org/10.1021/acs.nanolett.2c01757
Nano Lett. 2022, 22, 6235−6244

Supplementary Information for:

Ultra-photostable DNA FluoroCubes: mechanism of photostability and compatibility with FRET and dark quenching

Aaron T. Blanchard[1,2,3,†], Zi Li[1,‡], Elizabeth C. Duran[1], Catherine E. Scull[1], J. Damon Hoff[4], Keenan R. Wright[5], Victor Pan[6,§], Nils G. Walter[1,7,*]

[1]Single Molecule Analysis Group, Department of Chemistry, University of Michigan, Ann Arbor, Michigan, 48109, United States

[2]Department of Biomedical Engineering, University of Michigan, Ann Arbor, Michigan, 48109, United States

[3]Michigan Society of Fellows, University of Michigan, Ann Arbor, Michigan 48109, United States

[4]Single Molecule Analysis in Real-Time (SMART) Center, University of Michigan, Ann Arbor, Michigan 48109, USA

[5]Department of Chemistry, University of Michigan, Ann Arbor, Michigan, 48109, United States

[6]Department of Biomedical Engineering, Emory University and the Georgia Institute of Technology, Atlanta, Georgia, 30322

[7]Center for RNA Biomedicine, University of Michigan, Ann Arbor, Michigan, 48109, United States

† Current address: Department of Biomedical Engineering, Duke University, Durham, North Carolina, 27705, United States

‡ Current address: Pacific Biosciences, Menlo Park, California, 94025, United States

§ Current address: Intellia Therapeutics, Cambridge, Massachusetts 02139, United States

* Address Correspondence To: nwalter@umich.edu

Contents

I. Methods

Materials

All reagents for preparing buffers were purchased from Sigma-Aldrich or Thermo-Fisher and used without further purification. All dilutions and were performed in Milli-Q ultrapure water (henceforth referred to simply as water). All oligonucleotides were purchased from Integrated DNA Technologies (IDT – Iowa, USA), diluted to 100 μm in water, and used without further purification. Oligonucleotides labeled with fluorophores and/or quenchers were purchased from IDT with HPLC purification, and all others were purchased with standard desalting.

Design of FluoroCubes

The Cy3 FluoroCube strand sequences used in this work were taken directly from previous work[1] and are shown in Table S1. Dyes that were removed (for studies of FluoroCubes with fewer than 6 dyes) were replaced with 4T overhangs to inhibit end-to-end stacking interactions between FluoroCubes. The 2-strand FluoroCube was designed by first determining a routing diagram (Figure S3a) that could conceivably produce a stable rectangular prism 4-helix bundle from two 32 nt oligonucleotides. Once the routing diagram was determined, a MATLAB script was used to determine which oligonucleotide sequence could fold with strand A to achieve the desired routing. Poly-T loops were added because the routing diagram is sterically hindered. The Cy5 FluoroCube used in this work was designed by taking the Cy3 FluoroCube strands and swapping all A bases with G bases and swapping all T bases with C bases, and vice-versa. While this design was suitable for this work, for future studies we recommend against using these sequences because they contain high GC content, which may result in low folding yield. The fluorogenic sequence was designed for a different research project to possess no predicted secondary structure using a MATLAB-based screening algorithm. This algorithm will be presented in a later manuscript.

FluoroCube assembly and agarose gel purification

FluoroCubes were assembled and purified as previously described[1]. Briefly, FluoroCube strands were mixed to a final, equimolar concentrations of 2-10 μM in folding buffer (5 mM Tris pH 8.5, 1 mM EDTA and 40 mM $MgCl_2$). Annealing was performed in a Nexus thermocycler (Eppendorf) by denaturation at 85 °C for 5 min followed by cooling from 80 to 65 °C at a rate of 1 °C per 5 min, followed by cooling from 65 to 25 °C at a rate of 1 °C per 20 min. Following this process, samples were held at 4 °C. Within less than three hours, samples were mixed with ~10 μL of a 50-50 (w/w) loading mixture of glycerol and water and immediately loaded into wells of a 3% (or 4% where noted) agarose gel in 1x TBE with 12 mM $MgCl_2$ in a 4 °C cold room. Agarose gel electrophoresis was then run for 3 hours (unless otherwise indicated) at 70 V in the cold room. The gels were scanned using a Typhoon 410 Variable Mode Imager (GE Healthcare) operating in fluorescence mode. The PMT voltage was calculated via the "auto-PMT" feature based on pre-scans. FluoroCube-rich regions of the gel could be seen by eye due to Cy3 light scattering and absorbance, and were excised with razor blades and placed into Freeze n' Squeeze tubes (Bio-Rad Sciences, 732-6165) for purification. Purified FluoroCube absorbance spectra were measured using a Nanodrop spectrophotometer with the "microarray" setting, and the absorbance at 260 nm (A_{260}) was used as a measure of concentration. Purified FluoroCubes were kept at 4 °C (in 1x TBE with 12 mM $MgCl_2$) for up to six months before use.

Preparation of surfaces and sample cells

Surfaces and sample cells were constructed as previously described[2-4]. Briefly, glass coverslips were prepared via 3 steps: 1) VWR No. 1.5, 24×50 mm coverslips (VWR, catalog no. 48393-241) were cleaned via 3 min of plasma etching, followed by two rinses with acetone. 2) Cleaned coverslips were then mounted in a Coplin jar and aminated via incubation at room temperature in a 3% v/v solution of (3-aminopropyl) triethoxysilane (APTES) (Sigma-Aldrich, catalog no. A3648-100ML) in acetone, followed

by a 1 min sonication and another 10 min incubation at room temperature. 3) Aminated coverslips were subsequently passivated by sandwiching 80-100 µL of a 1:100 mixture of biotin-PEG-5000 (0.0025 mg/mL) and mPEG-5000 (0.25 mg/mL Laysan Bio, Inc.) in 0.1 M sodium bicarbonate between pairs of coverslips (generally, coverslips were prepared in batches of 8) and incubating at room temperature overnight in the dark. The slides were then rinsed under a stream of water and further passivated by sandwiching 80-100 µL of 0.03 mg/µL disulfosuccinimidyltartrate (DST, Soltec Ventures, catalog no. CL107) in 1M sodium bicarbonate between pairs of coverslips and incubating at room temperature in the dark for 30 min. Passivated coverslips were then stored for up to 2 months in the dark at -20 °C.

To construct sample cells, 100 µL pipet tips were cut to a length of ~2 cm as measured from the wide end, and the noncut base was adhered to a passivated glass coverslip via epoxy (Hardman Double/Bubble #04001). In this manner, 6-8 sample cells could be attached to each coverslip. Sample cells were then washed 3× in 1×phosphate buffer saline (1×PBS). Each sample cell "wash" entails pipetting ~200 µL of solution into the sample cell, then slowly pipetting the full solution up and down 3× before discarding the wash solution. Sample cells were then incubated for ~10 min with 0.01 mg/mL streptavidin in 1× PBS and subsequently washed 3× in 1×PBS and 1× in FluoroCube buffer. FluoroCube buffer consists of 20 mM Tris pH 8.0, 1 mM EDTA, 20 mM $MgCl_2$ (note that previous work[1] used 20 mM Mg-Acetate instead of $MgCl_2$) and 50 mM NaCl. Biotin-labeled FluoroCubes were then incubated in sample cells for 5 min at an effective concentration of A_{260}=2.5 × 10^{-6} (however, this incubation time and concentration was adjusted from experiment to experiment to achieve surface densities that were acceptable for single molecule photobleaching experiments) and subsequently washed 5× in FluoroCube buffer. These samples were then used for imaging experiments on the same day and/or stored at 4°C in the dark for up to two weeks. For experiments performed on subsequent days, sample cells were washed 3× in FluoroCube buffer before imaging.

Single molecule imaging and analysis

The vast majority of single molecule photobleaching data in this work was collected on the single particle tracker (SPT) microscope housed in the Single Molecule Analysis in Real-Time (SMART) Center at the University of Michigan. Some additional studies (specifically, the images shown in Figure 1 d&e and the 2-strand FluoroCube data shown in Figure S3, as well as preliminary trials not published here) were performed on the Oxford Nanoimager (ONI) microscope housed in the Walter lab at the University of Michigan.

The SPT has an IX-81 computer-controlled Olympus microscope body. For these studies, a 100× oil 1.4NA (UPLSAPO100XO) objective was used, along with a quadband dichroic (Chroma) with 405/488/561/640 pass bands and a Sapphire 561-50 CW laser operated at 100% power (~50 mW at the laser head). The laser power through-the-objective was measured on the day of each experiment using a handheld power meter with the laser oriented in epifluorescence mode. Typical power measurements were between 7 and 11 mW. The total spot size of the laser is ~400 um in diameter, corresponding to an excitation laser power density (with 10 mW total) of ~8 W/cm^2. A Cell^TIRF (Olympus) module was used to orient the excitation laser in total internal reflection fluorescence (TIRF) mode with a penetration depth of 110 nm. An Olympus ZDC2 z-drift control module was used to prevent loss of focus during image acquisition.

The ONI is a Nanoimager S with 405 nm, 473 nm, 532 nm, and 640 nm lasers and a 640 nm dichroic that splits emission to separate paths to two cameras. For this study, the 532 nm laser (100 mW max power at the laser head) was used at a 30 mW setting in TIRF mode. The emission light in this microscope passes through a 550-620 nm bandpass filter before reaching the camera. While the fraction of laser power that passes from the laser to the sample is expected to be high, the intensity of light leaving the laser fluctuates over ~min timescales, meaning that not all experiments performed on this microscope were conducted stably at 30 mW. As such, the ONI data (Figure S3 and the images in Figure 1 d-e) were only suitable for visual display and the estimation of the total number of detected photons ($N_{photons}$).

Generally, surfaces were focused upon manually and the z-drift control system was activated to obtain stably in-focus FluoroCubes. The laser was then de-activated and the stage was moved laterally to

an area of the sample well that had not previously been exposed to the excitation laser. Digital control of the laser was then used to activate the laser immediately prior to the commencement of a 10-min acquisition. Videos were collected as stream acquisitions with 500 ms frames. Three videos of one sample well were generally collected serially using automated stage shifting between videos. Imaging was performed in two different conditions, denoted +OSS or -OSS. The +OSS condition was performed in 0.89x FluoroCube buffer with an oxygen scavenger system (OSS) consisting of 1 mM Trolox, 5 mM protocatechuic acid (PCA), and 50 nM protocatechuate-3,4-dioxygenase (PCD). The -OSS condition consisted of 1x FluoroCube buffer.

Measurement and analysis of fluorescence lifetime and fluorescence anisotropy

Fluorescence lifetime and fluorescence anisotropy measurements were collected on an Alba time-resolved confocal fluorescence microscope (ISS Inc.) equipped with an IX-81 Olympus microscope body, a U-Plan S-APO 60X water immersion objective (1.2 NA, 0.28 mm working distance), an SPC-830 time-correlated single photon counting board (Becker & Hickl), an SC-400-8-PP Super-continuum laser (Fianium), and two cooled, low-noise avalanche photodiodes. At least three replicates were collected for each experiment. FluoroCubes (and free Cy3 controls) were excited with linearly polarized 561 nm light using a Fianium WhiteLase supercontinuum laser with an acousto-optic tunable filter for wavelength selection. Picosecond laser pulses were applied to the sample at 20 MHz for 5 minutes per acquisition. Fluorescent emission was filtered through a 593/40 bandpass filter and split by a polarizing beam-splitting cube between two photodiode acquisition channels (the $I_{\parallel}$ channel, which is polarized parallel to the excitation light, and the $I_{\perp}$ channel, which is polarized perpendicular to the excitation light). The instrument response function (IRF) of each detection channel was measured by placing a mirror above the objective and recording the time-resolved response from reflected 561nm photons.

Prior to image collection, 6-dye FluoroCubes were imaged under different excitation powers, and the highest power that didn't appear to cause substantial photobleaching in the time that single FluoroCubes diffuse through the confocal volume was used for all subsequent experimentation. The confocal volume has a radius of ~280 nm and a total power of ~20 uW, resulting in an excitation laser power density of ~8,000 W/cm^2.

Sample cells were prepared by oxygen-plasma cleaning coverglass (to limit non-specific adsorption of FluoroCubes to the glass surface) and affixing pipette tips to the glass as described above. Samples were diluted to an A_{260} nm absorbance of 0.00005 in 1x FluoroCube buffer before acquisition with 0.05% (w/v) Tween-20 (which also helps to limit nonspecific absorption to the coverglass). When stated, the experimental buffer also included an OSS consisting of 1 mM Trolox, 5 mM PCA, and 50 nM PCD. For non-OSS samples, the volume of PCA/PCD/Trolox was replaced by deionized water. The time resolved fluorescence anisotropy measurements were also performed in 1x FluoroCube buffer with 30% (by volume) glycerol. We added glycerol to slow the FluoroCubes' rotation to better assess the effect of homoFRET on anisotropy decay.

Analysis of fluorescent lifetime was performed using custom-written MATLAB scripts. Histograms of arrival times were calculated, and fluorescence lifetimes were fit to histograms using the tail-fit method (e.g. ignoring the early, sub ~300 ps post-pulse time-points that are often distorted due to overlap with the IRF). We fit all histograms with mono-, bi-, and tri-exponential decay functions and found that bi-exponential decay was much more accurate than mono-exponential decay and roughly as accurate as tri-exponential decay. Therefore, we calculated fluorescence lifetime by taking the weighted average of the lifetimes in the two exponentials from the bi-exponential decay fit.

The Isotropic brightness (I_{iso}) of the sample (figure S15b, top) was calculated as

$$I_{iso} = I_{\parallel} + 2GI_{\perp}$$

where G is the G-factor estimated as the ratio of $I_{\parallel}/I_{\perp}$ measured using freely-diffusing Atto488 dye. The fluorescence anisotropy (r) was calculated as

$$r = \frac{I_{\parallel} - GI_{\perp}}{I_{iso}}$$

For the steady-state fluorescence anisotropy calculation, these calculations were performed with $I_{\perp}$ and $I_{\parallel}$ as the total number of photons counted in each of the two channels. The time resolved fluorescence anisotropy, $r(t)$, was calculated as a function of time by binning occurrences by arrival time and calculating the anisotropy for each bin with the equation above. Equation 3 in the main text was then fit to $r(t)$ vs t for each sample using custom MATLAB code (via MATLAB's "fminsearch" function) with IRF deconvolution.

In solution fluorogenicity measurements

Fluorogenicity was measured using an ID3 plate reader (Molecular Devices, San Jose, CA, USA). Briefly, 100 µL of fluorogenic FluoroCube in 1x TBE with 12 mM $MgCl_2$ at A_{260}=0.01 (or, as a control, 100 nM fluorogenic probe in 4x PBS) was added to each imaging well in a 96-well plate. The-96 well plate was then inserted into the plate reader, and all wells were imaged in the "fluorescence" mode with low EMT gain, a 100 ms integration time, a read height of 1 mm, and excitation/emission wavelengths of 540/570 (Cy3) and 640/670 (Cy5). All wells in the experiment, as well as a negative control well with buffer only, were imaged at ~1-min intervals for ~10 min. Then, 1 µL of 100 µM full complement was added to each well to achieve a final concentration of 1 µM. Fluorescence intensity was again recorded at 1-min intervals for 30+ min to allow the in-solution intensity to plateau. The fluorescence intensity vs. time data for each well was then exported as an Excel table, loaded in MATLAB, baseline subtracted (using the negative control) and then divided by the initial intensity (I_0, calculated by averaging the 11 intensity measurements taken before the addition of the full complement) to obtain I/I_0. Fluorogenicity was then defined as the maximum I/I_0 measured from throughout the timelapse (Figure 3e).

In-gel measurement of effective FRET efficiency

Agarose gels containing FluoroCubes for FRET experiments (Figures 4, S18-19) were imaged using a Typhoon 410 Variable Mode Imager (GE Healthcare) operating in Fluorescence mode. A sensitized emission acquisition, consisting of one image with Cy3 emission and excitation filters (I_{Cy3}), one image with Cy5 emission and excitation filters (I_{Cy5}), and one with the Cy3 excitation filter and the Cy5 emission filter (I_{FRET}). This process cannot be used to directly calculate FRET efficiency. Instead, the effective FRET efficiency (E_{eff}), which is linearly proportional to the number of complexes exhibiting FRET, was calculated and compared between conditions. E_{eff} was calculated as:

$$E_{eff} = \frac{I_{sens}}{I_{Cy5}}$$

where the sensitized emission image (I_{sens}) is:

$$I_{sens} = I_{FRET} - dI_{Cy3} - aI_{Cy5}$$

The bleed-through coefficients d and a were calculated by measuring I_{FRET}/I_{Cy3} of a Cy3-only sample and by measuring I_{FRET}/I_{Cy5} of a Cy5-only sample (both imaged within the same gel), respectively (Figure S18). To compare FRET between conditions, E_{eff} was integrated along gel lanes.

Data processing

Data processing was performed in MATLAB 2020b, with some preliminary image viewing in Fiji (an enhanced version of ImageJ, version 1.53f51) and fluorogenic data storage in Microsoft Excel. Figures were prepared in Adobe Illustrator CC 2019. Single molecule photobleaching studies were processed using an automated process shown in Figure S2. Curve fitting to single molecule photobleaching data was performed using MATLAB's built-in "fit" command (for single molecule photobleaching studies). Curve fit confidence intervals shown in Figure 1 h&i were obtained using MATLAB's built-in "predint" function with the simultaneous and functional options set. Correlations were performed using the corrcoef command. $N_{photons}$ was calculated from best-fit parameters A/k_1. Statistical comparisons were conducted using t-tests and Pearson's correlations unless stated otherwise. FRET FluoroCube data were processed using a pipeline shown in Figure S18. Fluorescence lifetime and anisotropy data processing was performed in MATLAB as described in the methods sub-section "**Measurement and analysis of fluorescence lifetime and fluorescence anisotropy**" above.

II. Supplementary Figures

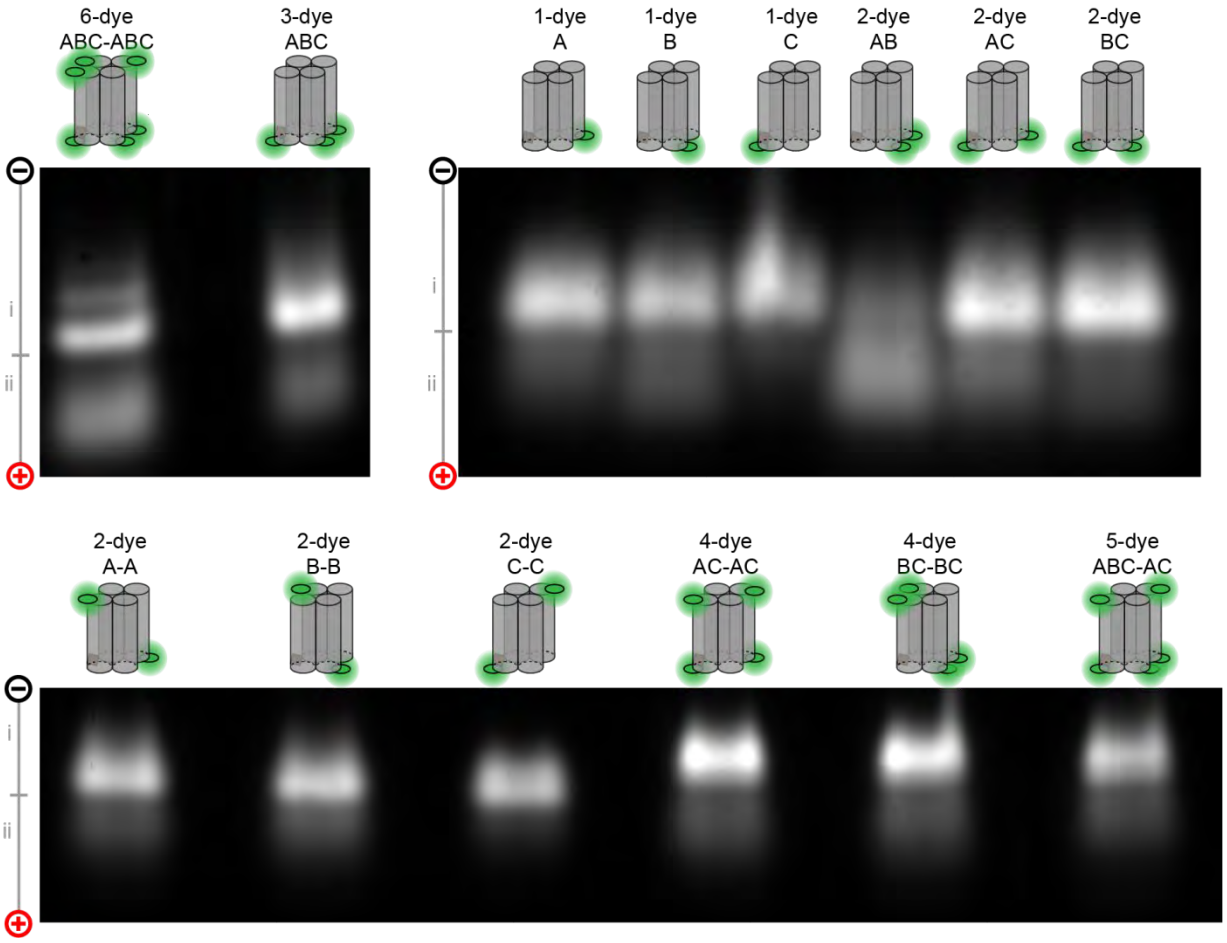

Figure S1: Fourteen FluoroCube constructs and purification
Schematic depictions and excerpts of Cy3 fluorescence images taken of 3% agarose gels post-electrophoresis for the 14 constructs used in this work. In all cases electrophoresis was performed directly following assembly. All gel images are labeled on the left with a + and – end showing that the direction of flow was from top (-) to bottom (+) in the image. A dividing line shows the approximate flow coordinates that were generally interpreted as containing assembled FluoroCubes (i) or incomplete FluoroCubes and un-assembled single strands (ii). Examples of gels with lanes containing only single-stranded DNA can be found in Figures S3 and S17. Following collection of these images, bands expected to contain assembled FluoroCubes were cut out using a razor blade and transferred to Freeze N' Squeeze tubes for purification.

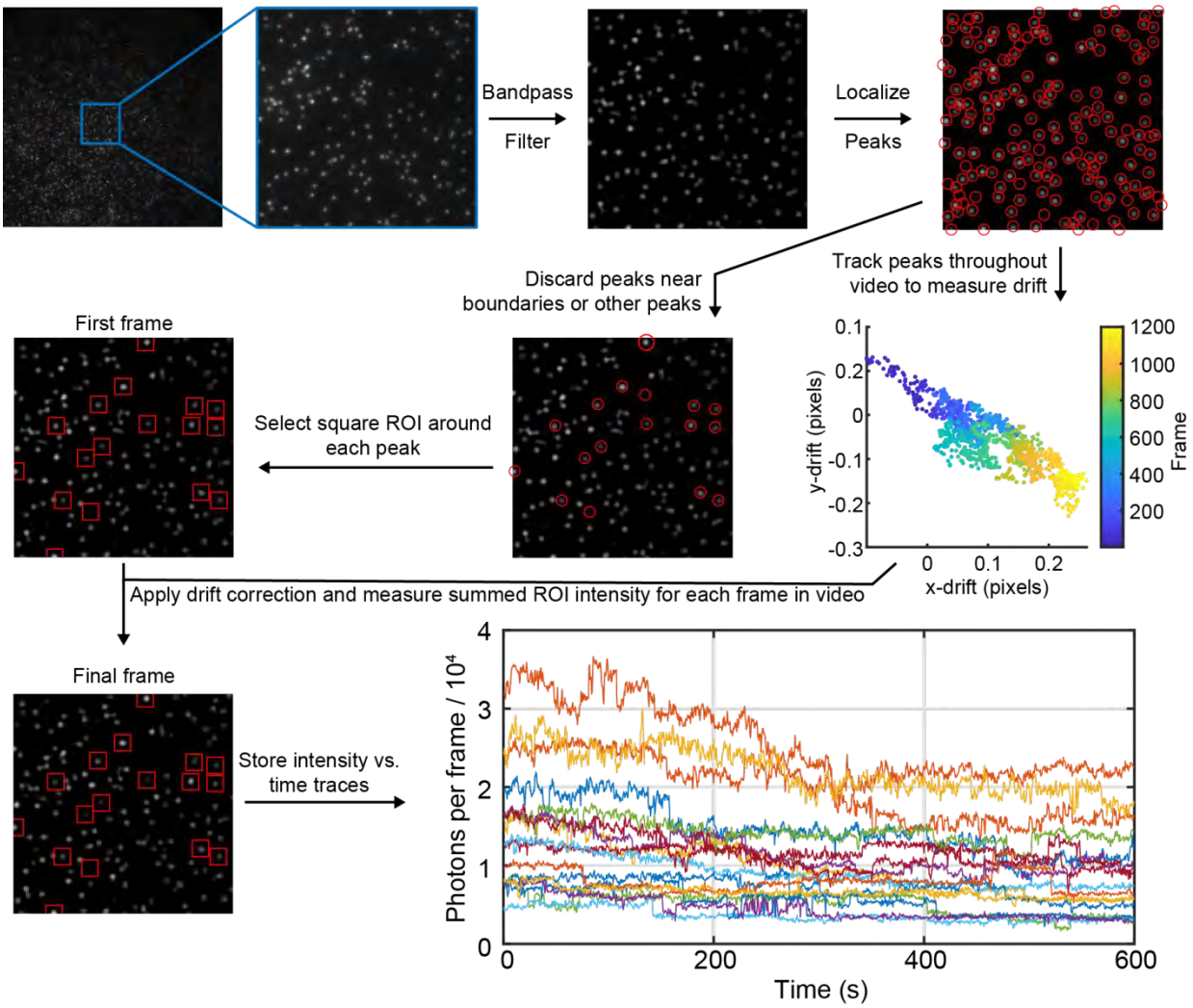

Figure S2: Single molecule photobleaching experiment pipeline
The top left shows the first full frame from a photobleaching experiment video (taken of 4-dye BC-BC FluoroCubes). Bandpass, peak localization, and peak tracking functions were taken from the IDL particle tracker software[5] (adapted for MATLAB by Daniel Blair and Eric Dufresne). First, a bandpass function is used to remove low- and high-frequency noise from the image. Bandpass lower and upper bounds were set to 1 pixel (the typical length scale of high-frequency noise) and 5 pixels (roughly the width of a single molecule point spread function), respectively. Next, peaks are localized in each frame and used to measure drift via trajectory averaging. Next, the peaks for the first frame were parsed to exclude peaks that were within ~10 pixels of an image border or other peaks. A square ROI was drawn around each remaining peak, and the summed intensity of each ROI was taken in each frame to obtain the particle's intensity vs. time trace. The large heterogeneity in brightness observed between FluoroCubes is typical for FluoroCubes.[1]

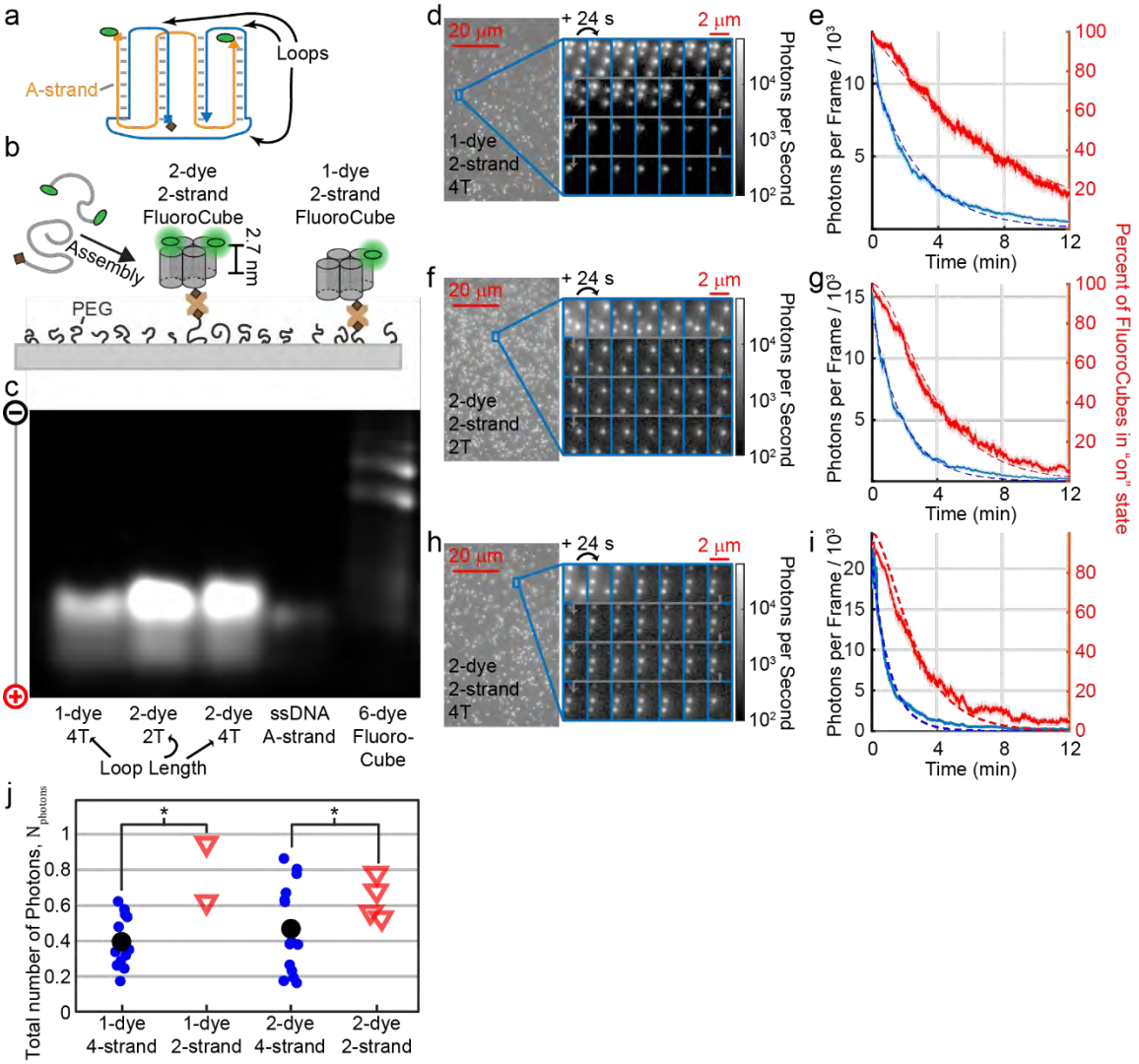

Figure S3: 2-strand FluoroCube design, purification, and on-surface photobleaching
a) A routing diagram showing the design of the 2-strand FluoroCube, which is assembled using the A strand from the standard FluoroCube and a second strand that has been specially designed to achieve this routing. 2T or 4T loops were used to enable assembly despite the sterically-hindered design. A similar routing diagram for the 4-strand FluoroCube can be found in the original FluoroCube manuscript.[1] **b)** Schematic depiction of the assembled, surface-captured constructs. **c)** Cy3 fluorescence image of a 4% agarose gel with 2-strand FluoroCubes and, for reference, single stranded A strands and 6-dye, 4-strand FluoroCubes. The two strand FluoroCubes appear to exhibit very similar, but noticeably lower, mobility to the ssDNA. **d)** Initial frame from a video of single molecule photobleaching of 1-dye 2-strand FluoroCubes with 4T loops. A zoomed-in region is shown for 28 frames taken at 24-second intervals throughout the video. Note the logarithmic scale of the intensity scale bar. **e)** Average photon count (left y-axis scale, blue curves) and percent of unbleached FluoroCubes (right y-axis scale, red curves) with dashed line fits for the 1-dye 2-strand FluoroCubes with 4T loops. **f, g)** same as **d** and **e**, but for 2-dye 2-strand FluoroCubes with 2T loops. **h, i)** Same as **d** and **e**, but for 2-dye 2-strand FluoroCubes with 4T loops. **j)** Statistical comparisons (two-sided student's t-test) between N_{photon} values measured for 2-strand and 4-strand FluoroCubes. * denotes $p<0.05$. Blue dots and red-triangles denote N_{photon} values from individual videos, while the black dots show averages across all 4-strand experiments. The two design types were imaged on different microscopes.

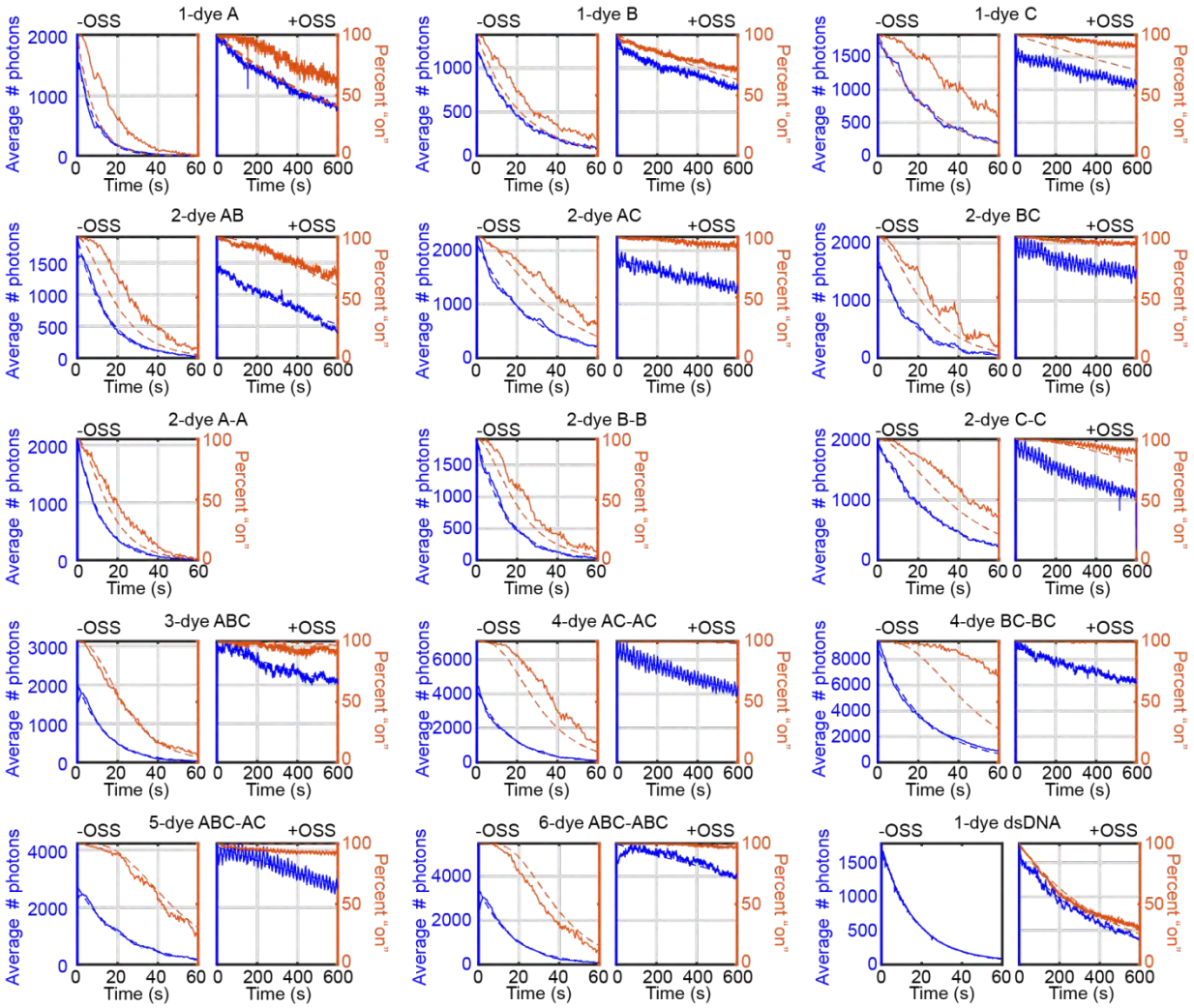

Figure S4: Single-exponential decay model fits to data from single molecule photobleaching experiments

Each plot shows the average photon count (left y-axis scale, blue curves) and percent of unbleached FluoroCubes (right y-axis scale, red curves) with dashed line fits from a single video. One representative plot is shown for each of the 14 FluoroCube constructs studied in this work with or without the PCA/PCD oxygen scavenging system (OSS) and Trolox, as indicated by annotations above each plot. Solid curves show data, while dashed curves show fits obtained by fitting to equation (1) from the main text using the average photon count per FluoroCube per frame vs. time. Fit curves are also shown for the percent of unbleached FluoroCube plots to illustrate the accuracy with which the average intensity fit reports on the fraction of remaining unbleached FluoroCubes. Data with OSS are not shown for 2-dye A-A or 2-dye B-B because the relevant datasets were not suitable for final use (specifically, following culmination of this study, the surface densities in B-B and A-A +OSS acquisitions were determined to be too high for single molecule imaging). Some data curves exhibit small, high frequency intensity oscillations. These oscillations are the result of small errors with the microscope's auto-focus system, which are not expected to affect experimental results. An additional pair of plots is shown for experiments with single dyes attached to individual DNA duplexes (specifically, the 5'-labeled A strand was captured on the surfaces to match previously-performed experiments[1]). Note that photobleaching of the 1-dye dsDNA construct without OSS (bottom plot, second from the right) was performed using 50 ms exposure time (compared to 500 ms for

the single FluoroCube photobleaching experiments) on a dense field of dsDNA. Accordingly, this condition does not reflect single molecule photobleaching data, and the intensity vs. time and fit curves show the average intensity of the field of view, with a y-axis that ranges from 0 to 3,000 arbitrary units.

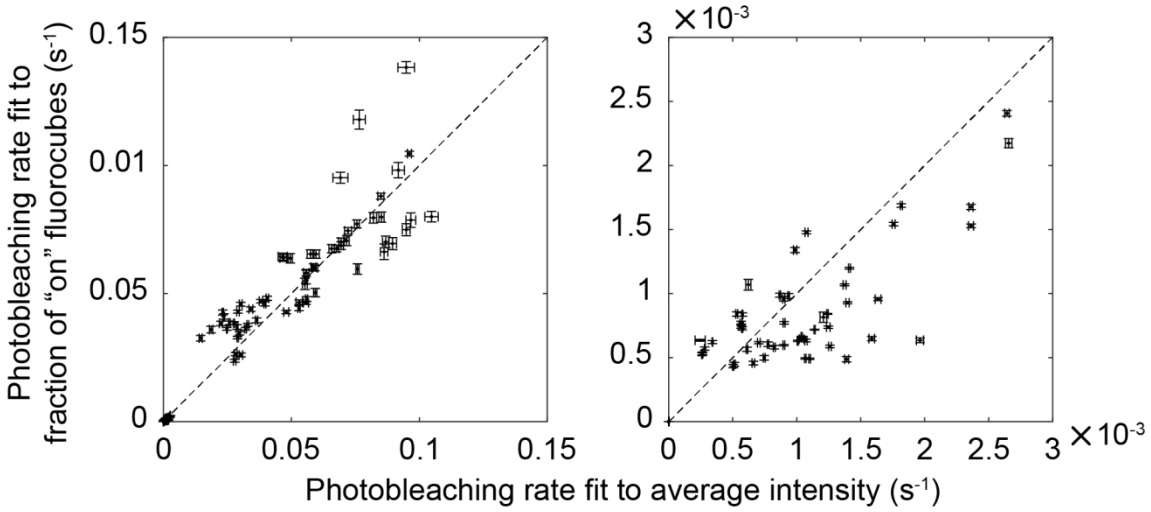

Figure S5: Correlation between best-fit k_1 values obtained from two different fit types for single molecule photobleaching studies

Plot of k_1 measured by fitting to average intensity vs. time (main text equation 1) or fraction of remaining unbleached FluoroCubes (main text equation 2). Each data point corresponds to one experimental video, and errorbars show the 95% confidence interval of the k_1 fit parameter. The right plot is a zoom-in on the bottom left corner of the left plot, and generally portrays the +OSS data while the left plot primarily portrays the -OSS data. The two fitting methods appear to produce highly correlated results (correlation coefficient: 0.88) that are clustered around the y=x line (dashed).

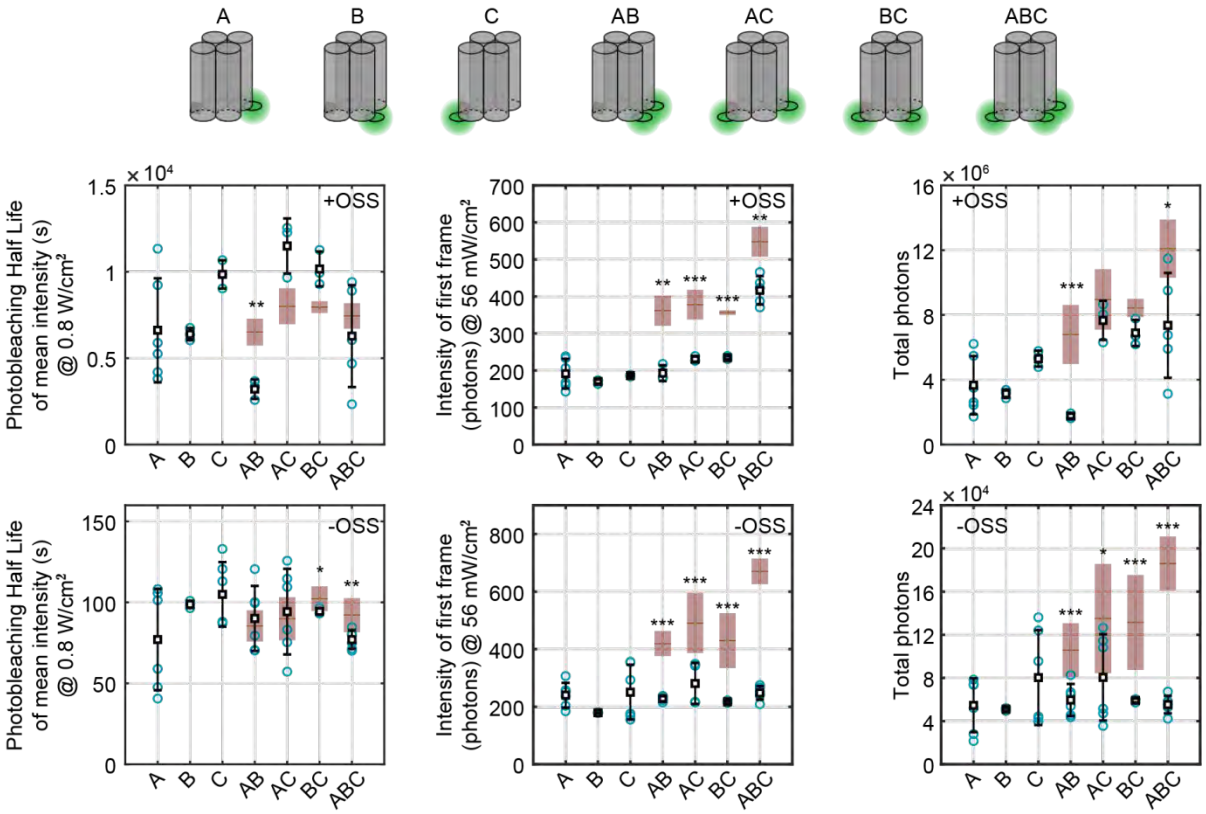

Figure S6: Fit parameters from single-molecule photobleaching studies show sub-linear scaling of brightness and total photon count.

Schematics of the seven FluoroCube constructs with fluorophores all on one side of the FluoorCube are shown on the top. Plots showing the average photobleaching half-life ($1/k_1$ - left), intensity of the first frame (A - middle), and total photons ($N_{photons}$ – right), with OSS (top row) and without OSS (bottom row) measured from single molecule photobleaching experiments are shown for each of the seven constructs. Blue circles show the results from individual videos, black squares and errorbars show the average and standard deviation of the single-video fit results, and grey lines and red shading show the average and standard deviation that would be expected from linear addition of fluorescence from the individual dyes. Asterisks above shading denote the results of student's t-tests comparing the measurements to the averages calculated from linear addition, with * denoting p<0.05, ** denoting p<0.01, and *** denoting p<0.001.

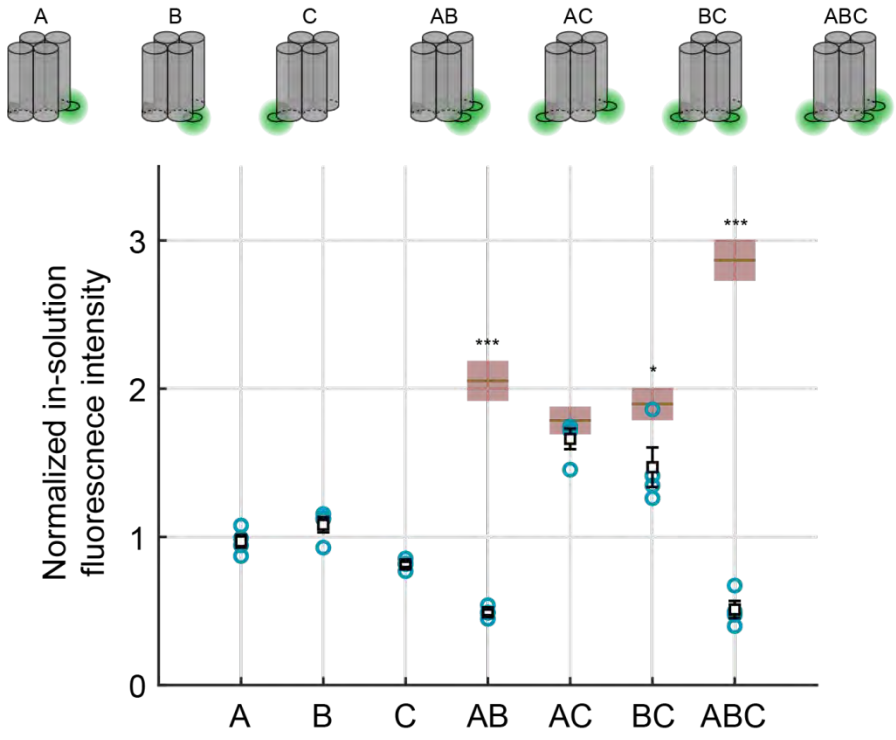

Figure S7: Sub-linear scaling of FluoroCube brightness in solution
Schematics of the seven FluoroCube constructs with fluorophores on one side are shown on the top. A plot showing the average in-solution fluorescence intensity for each of the seven constructs is shown below. Blue circles show the results from four individual experiments, black squares and errorbars show the average and standard deviation of single-experiment results, and grey lines and red shading show the average and standard deviation that would be expected from linear addition of fluorescence from the individual dyes. Asterisks above shading denote the results of student's t-tests comparing the measurements to the averages calculated from linear addition, with * denoting $p<0.05$, ** denoting $p<0.01$, and *** denoting $p<0.001$. These experiments were performed at approximately equivalent concentrations; they were diluted such that the absorbance at 260 nm would be equal to 0.01.

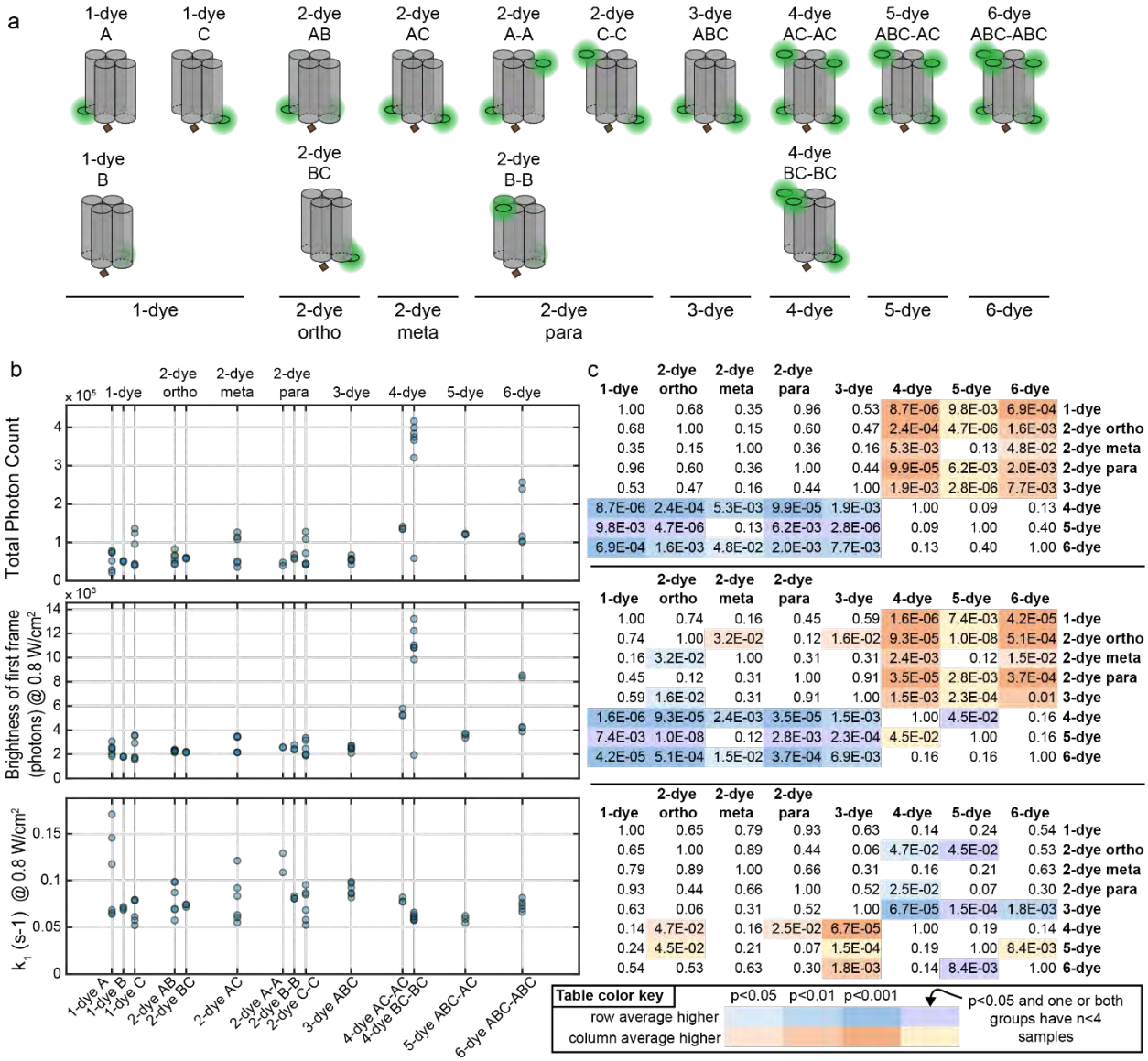

	1-dye	2-dye ortho	2-dye meta	2-dye para	3-dye	4-dye	5-dye	6-dye
1-dye	1.00	0.68	0.35	0.96	0.53	8.7E-06	9.8E-03	6.9E-04
2-dye ortho	0.68	1.00	0.15	0.60	0.47	2.4E-04	4.7E-06	1.6E-03
2-dye meta	0.35	0.15	1.00	0.36	0.16	5.3E-03	0.13	4.8E-02
2-dye para	0.96	0.60	0.36	1.00	0.44	9.9E-05	6.2E-03	2.0E-03
3-dye	0.53	0.47	0.16	0.44	1.00	1.9E-03	2.8E-06	7.7E-03
4-dye	8.7E-06	2.4E-04	5.3E-03	9.9E-05	1.9E-03	1.00	0.09	0.13
5-dye	9.8E-03	4.7E-06	0.13	6.2E-03	2.8E-06	0.09	1.00	0.40
6-dye	6.9E-04	1.6E-03	4.8E-02	2.0E-03	7.7E-03	0.13	0.40	1.00

	1-dye	2-dye ortho	2-dye meta	2-dye para	3-dye	4-dye	5-dye	6-dye
1-dye	1.00	0.74	0.16	0.45	0.59	1.6E-06	7.4E-03	4.2E-05
2-dye ortho	0.74	1.00	3.2E-02	0.12	1.6E-02	9.3E-05	1.0E-08	5.1E-04
2-dye meta	0.16	3.2E-02	1.00	0.31	0.31	2.4E-03	0.12	1.5E-02
2-dye para	0.45	0.12	0.31	1.00	0.91	3.5E-05	2.8E-03	3.7E-04
3-dye	0.59	1.6E-02	0.31	0.91	1.00	1.5E-03	2.3E-04	0.01
4-dye	1.6E-06	9.3E-05	2.4E-03	3.5E-05	1.5E-03	1.00	4.5E-02	0.16
5-dye	7.4E-03	1.0E-08	0.12	2.8E-03	2.3E-04	4.5E-02	1.00	0.16
6-dye	4.2E-05	5.1E-04	1.5E-02	3.7E-04	6.9E-03	0.16	0.16	1.00

	1-dye	2-dye ortho	2-dye meta	2-dye para	3-dye	4-dye	5-dye	6-dye
1-dye	1.00	0.65	0.79	0.93	0.63	0.14	0.24	0.54
2-dye ortho	0.65	1.00	0.89	0.44	0.06	4.7E-02	4.5E-02	0.53
2-dye meta	0.79	0.89	1.00	0.66	0.31	0.16	0.21	0.63
2-dye para	0.93	0.44	0.66	1.00	0.52	2.5E-02	0.07	0.30
3-dye	0.63	0.06	0.31	0.52	1.00	6.7E-05	1.5E-04	1.8E-03
4-dye	0.14	4.7E-02	0.16	2.5E-02	6.7E-05	1.00	0.19	0.14
5-dye	0.24	4.5E-02	0.21	0.07	1.5E-04	0.19	1.00	8.4E-03
6-dye	0.54	0.53	0.63	0.30	1.8E-03	0.14	8.4E-03	1.00

Figure S8: Quantification of single-molecule photobleaching metrics and statistical comparisons between constructs: without OSS

a) Illustrations of the 14 constructs used in this work. For the purpose of statistical comparisons, the constructs are sorted into 8 groups with between 1 and 3 constructs each, as shown. These groups include: 1-dye, which includes the 3 constructs with a single dye (1-dye A, 1-dye B, and 1-dye C); 2-dye ortho, which includes the two constructs with two dyes on adjacent helices on the same side of the FluoroCube (2-dye AB and 2-dye BC); 2-dye meta, which contains the construct with two dyes on the same side of the FluoroCube on juxtaposed helices (2-dye AC); 3-dye (3-dye ABC); 4-dye (4-dye AC-AC and 4-dye BC-BC); 5-dye (5-dye ABC-AC); and 6-dye (6-dye ABC-ABC). **b)** Three plots show data points (blue circles) from individual single molecule photobleaching experiment measurements of $N_{photons}$ (top), the brightness of the first frame (middle), and the per-dye photobleaching rate k_1 (bottom) for each of the 14 constructs. Groups of constructs are clustered together. **c)** Tables of p-values from student's t-test comparisons between groups illustrated in corresponding plots in **b**. Each table entry shows the p-value for the comparison between the constructs indicated in the entry's row and column. Entries with p-values below 0.05 are colored according to the table shown on the figure's bottom right. Due to the long imaging durations and instrument usage time limitations, not all constructs could be imaged on the same day. Even with

appropriate controls, it is possible that slight modifications to the microscope between experimental days resulted in slight systematic biases over time. Therefore, to prevent over-interpretation of slight systematic biases, we only performed comparisons between sets of measurements pooled from groups of constructs. As a general trend, groups with n<4 dyes appear to exhibit similar brightness and $N_{photons}$ to each other, groups with n≥4 dyes appear to exhibit similar brightness and $N_{photons}$ to each other, and groups with n<4 dyes exhibit lower brightness and $N_{photons}$ than groups with n≥4. Few differences in k_1 were observed between groups, although notably the 3-dye FluoroCube construct appears to photobleach significantly faster than all of the groups with n≥4 dyes.

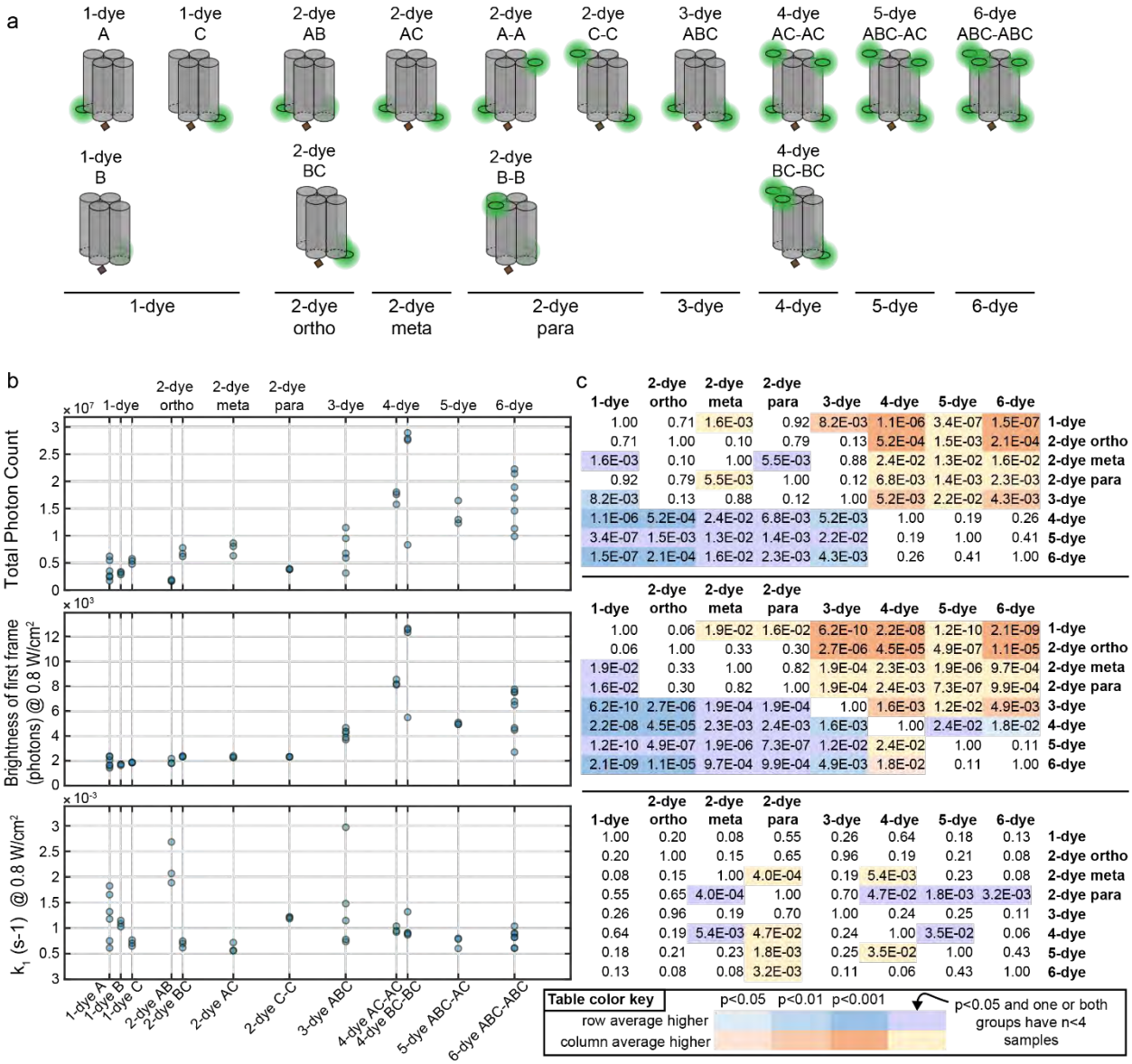

Figure S9: Quantification of single-molecule photobleaching metrics and statistical comparisons between constructs: with OSS

Same as the supplemental Figure S8, but with the addition of the PCA/PCD oxygen scavenging system and Trolox. **a)** Illustrations of the 14 constructs used in this work. For the purpose of statistical comparisons, the constructs are sorted into 8 groups with between 1 and 3 constructs each, as shown. These groups include: 1-dye, which includes the 3 constructs with a single dye (1-dye A, 1-dye B, and 1-dye C); 2-dye ortho, which includes the two constructs with two dyes on adjacent helices on the same side of the FluoroCube (2-dye AB and 2-dye BC); 2-dye meta, which contains the construct with two dyes on the same side of the FluoroCube on juxtaposed helices (2-dye AC); 3-dye (3-dye ABC); 4-dye (4-dye AC-AC and 4-dye BC-BC); 5-dye (5-dye ABC-AC); and 6-dye (6-dye ABC-ABC). **b)** Three plots show data points (blue circles) from individual single molecule photobleaching experiment measurements of $N_{photons}$ (top), the brightness of the first frame (middle), and the per-dye photobleaching rate k_1 (bottom) for each of the 14 constructs. Groups of constructs are clustered together. **c)** Tables of p-values from student's t-test comparisons between groups illustrated in corresponding plots in **b**. Each table entry shows the p-value for the comparison between the constructs indicated in the entry's row and column. Entries with p-values below

0.05 are colored according to the table shown on the figure's bottom right. Due to long imaging durations and instrument usage time limitations, not all constructs could be imaged on the same day. Even with appropriate controls, it is possible that slight modifications to the microscope between experimental days resulted in slight systematic biases over time. Therefore, to prevent over-interpretation of slight systematic biases, we only performed comparisons between sets of measurements pooled from groups of constructs. As a general trend, groups with n<4 dyes appear to exhibit similar $N_{photons}$ to each other, groups with n≥4 dyes appear to exhibit similar $N_{photons}$ to eachother, and groups with n<4 dyes exhibit lower $N_{photons}$ than groups with n≥4. A similar division was observed for the brightness data, with two notable differences: first, the 3-dye construct exhibited intermediate brightness, which was significantly lower than the n>4 constructs and significantly higher than the n<3 constructs; second, the 3-dye group exhibited significantly higher brightness than both the 5-dye and 6-dye constructs. Few differences in k_1 were observed between groups, except in cases where only 3 experimental measurements were included in one or both of the groups.

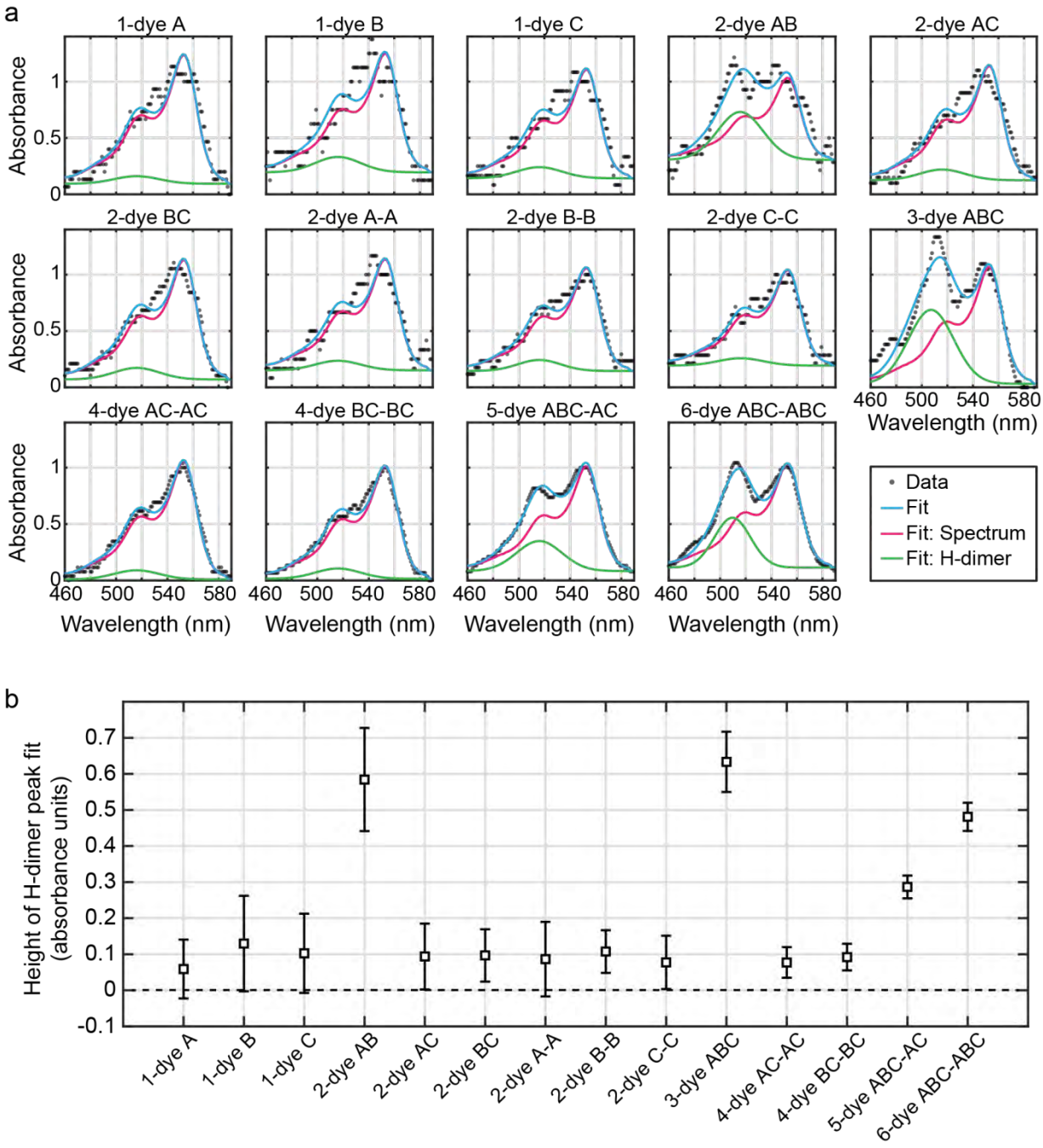

Figure S10: Quantification of H-dimerization via analysis of FluoroCube absorbance spectra
a) Fourteen plots are shown, one for each FluoroCube design. Each plot shows an absorbance spectrum of a single FluoroCube construct (black dots) along with a curve (blue) fit to the equation:

$$Absorbance = h_1 Absorbance_{Cy3}(\lambda) \; + \; h_2 \exp\left(-\left(\frac{\lambda - \lambda_0}{w}\right)^2\right) + b$$

where λ is wavelength, $Absorbance_{Cy3}(\lambda)$ is the peak-normalized Cy3 absorbance spectrum downloaded from the spectra viewer tool on Chroma.com, w and λ_0 are fit parameters for a Gaussian-shaped H-dimer peak, h_1 and h_2 are the maximum heights of the Cy3 spectrum and the H-dimer peak, respectively, and b is the baseline offset. For the fitting procedure, the fit parameters λ_0, w, h_2, h_1, and b, were given initial guesses of 511 nm, 10 nm, 0.1, and 1, and 0, respectively, lower bounds of 506 nm, 6 nm, -0.1, and 0.5, and -0.4, respectively, and upper bounds of 516 nm, 25 nm, 1, and 1.5, and 0.4, respectively. The H-dimer Gaussian component (green) and the Cy3 spectrum (magenta) portions of the fit are also graphically illustrated. **b)** The height of the H-dimer peak, normalized to the height of the Cy3 spectrum (e.g., h_2/h_1) is plotted for each construct, with errorbars representing the 95% confidence interval of the fit. Broadly speaking, the 2-dye AB, 3-dye ABC, and 6-dye ABC-ABC constructs exhibited high levels of H-dimerization, while the 5-dye construct exhibited an intermediate level of H-dimerization, and all other constructs exhibited low degrees of H-dimerization.

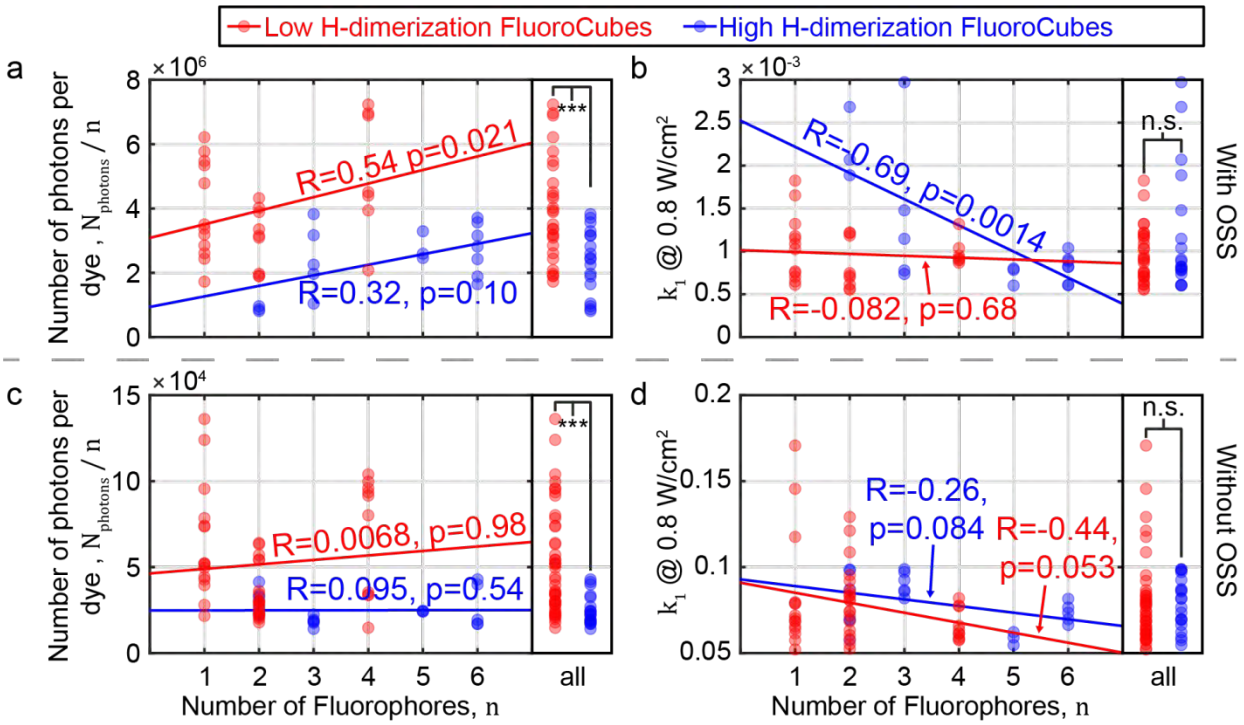

Figure S11: Trends among and comparisons between FluoroCubes with high and low extents of H-dimerization

Based on absorbance spectra shown in Figure S10, we divided FluoroCube constructs into a high H-dimerization group (2-dye AB, 3-dye ABC, 5-dye ABC-AC, and 6-dye ABC-ABC) and a low H-dimerization group (1-dye A, 1-dye B, 1-dye C, 2-dye AC, 2-dye BC, 4-dye AC-AC, and 4-dye BC-BC). We then analyzed trends within these two groups and performed comparisons between them in the presence (**a**, **b**) and absence (**c**, **d**) of the PCA/PCD oxygen scavenging system (OSS) and Trolox. Specifically, we measured the number of photons per dye (**a**, **c**) and the per-dye photobleaching rate constant k_1 (**b**, **d**). Each of the four plots in this subfigure shows individual data points (circles), colored by high- or low- H-dimerization group identity. Solid lines, also colored by group identity, show linear fits to the data points and are annotated with R and p values from Pearson's correlations between $N_{photons}/n$ or k_1 and n. The right side of each subfigure shows all points from the two groups grouped together for a single student's t-test comparison between the two groups. *** denotes p<0.001 and n.s. denotes p>0.05. The only statistically significant correlations observed were for 1) a negative correlation between k_1 and n for the high H-dimerization group in the presence of OSS (which may be caused solely by the high photobleaching rate of the 2-dye AB consturct), and 2) a positive correlation between $N_{photons}/n$ and n for the low H-dimerization group in the presence of OSS. Comparisons between groups showed that $N_{photons}/n$ was significantly higher – both in the presence and absence of OSS – for the low H-dimerization group than for the high H-dimerization group. Difference were not observed between groups for k_1. Together, these results suggest that H-dimerization undermines FluoroCube photon count by reducing instantaneous brightness and, in the case of low-n FluoroCubes, possibly by also accelerating the photobleaching process.

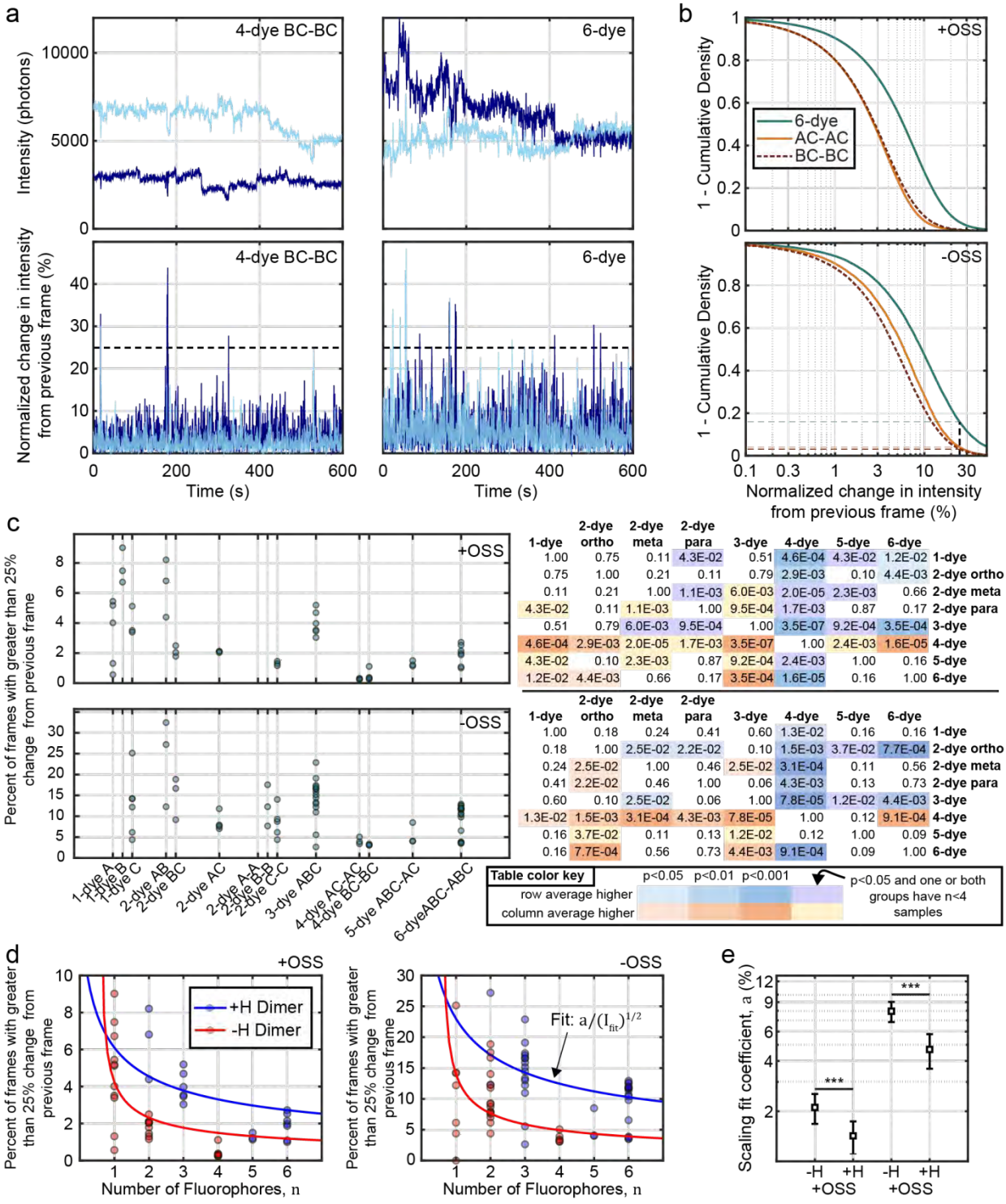

1-dye	2-dye ortho	2-dye meta	2-dye para	3-dye	4-dye	5-dye	6-dye	
1.00	0.75	0.11	4.3E-02	0.51	4.6E-04	4.3E-02	1.2E-02	1-dye
0.75	1.00	0.21	0.11	0.79	2.9E-03	0.10	4.4E-03	2-dye ortho
0.11	0.21	1.00	1.1E-03	6.0E-03	2.0E-05	2.3E-03	0.66	2-dye meta
4.3E-02	0.11	1.1E-03	1.00	9.5E-04	1.7E-03	0.87	0.17	2-dye para
0.51	0.79	6.0E-03	9.5E-04	1.00	3.5E-07	9.2E-04	3.5E-04	3-dye
4.6E-04	2.9E-03	2.0E-05	1.7E-03	3.5E-07	1.00	2.4E-03	1.6E-05	4-dye
4.3E-02	0.10	2.3E-03	0.87	9.2E-04	2.4E-03	1.00	0.16	5-dye
1.2E-02	4.4E-03	0.66	0.17	3.5E-04	1.6E-05	0.16	1.00	6-dye

1-dye	2-dye ortho	2-dye meta	2-dye para	3-dye	4-dye	5-dye	6-dye	
1.00	0.18	0.24	0.41	0.60	1.3E-02	0.16	0.16	1-dye
0.18	1.00	2.5E-02	2.2E-02	0.10	1.5E-03	3.7E-02	7.7E-04	2-dye ortho
0.24	2.5E-02	1.00	0.46	2.5E-02	3.1E-04	0.11	0.56	2-dye meta
0.41	2.2E-02	0.46	1.00	0.06	4.3E-03	0.13	0.73	2-dye para
0.60	0.10	2.5E-02	0.06	1.00	7.8E-05	1.2E-02	4.4E-03	3-dye
1.3E-02	1.5E-03	3.1E-04	4.3E-03	7.8E-05	1.00	0.12	9.1E-04	4-dye
0.16	3.7E-02	0.11	0.13	1.2E-02	0.12	1.00	0.09	5-dye
0.16	7.7E-04	0.56	0.73	4.4E-03	9.1E-04	0.09	1.00	6-dye

Figure S12: FluoroCube intensity fluctuations are linked to H-dimerization

a) (top) Two representative photon count per frame vs. time traces (light and dark blue curves, respectively) each for 4-dye BC-BC (top) and 6-dye ABC-ABC (right) FluoroCubes. (bottom) Relative

change in intensity for the corresponding photon count vs. time traces above. Relative intensity change for the i[th] frame (ΔI_i) is calculated from the intensity of frames i and $i-1$ as:

$$\Delta I_i = \frac{I_i - I_{i-1}}{(I_i + I_{i-1})/2} \times 100\%$$

b) Cumulative density functions of ΔI for the 4-dye and 6-dye FluoroCube constructs in the presence (top) and absence (bottom) of OSS. Note that only intensity vs. time traces from FluoroCubes that stayed bright for the entire duration of the video were included. In the bottom plot, interpolating lines show the calculation of the total fraction of frames in which $\Delta I > 25\%$. **c)** Two plots (left) show data points (blue circles) from individual single molecule photobleaching experiment measurements of ΔI in the presence (top) and absence (bottom) of OSS for each of the 14 constructs. Groups of constructs are clustered together. (right) Tables of p-values from student's t-test comparisons between groups illustrated in corresponding plots on the left. Each table entry shows the p-value for the comparison between the constructs indicated in the entry's row and column. Entries with p-values below 0.05 are colored according to the table shown on the figure's bottom right. Due to long imaging durations and instrument usage time limitations, not all constructs could be imaged on the same day. Even with appropriate controls, it is possible that slight modifications to the microscope between experimental days resulted in slight systematic biases over time. Therefore, to prevent over-interpretation of slight systematic biases, we only performed comparisons between sets of measurements pooled from groups of constructs. **d)** Individual data points (circles) from the plots **c**, colored by high- or low- H-dimerization group identity. Solid lines, also colored by group identity, show single parameter fits to the power law relationship

$$\Delta I = a_{fluc}/\sqrt{I_{fit}}$$

where a_{fluc} is the fit parameter and I_{fit} is a linear fit to the first-frame intensity vs n data ($I_{fit} = 957n + 236$ with H-dimerization, $I_{fit} = 2649n - 1526$ without H-dimerization – the same fit was used both with and without OSS because OSS was not show to substantially alter first-frame brightness, Figure S8-9). This inverse square-root fit approach was used because, due to the statistical nature of photon counting, intensity fluctuations are commonly known to intrinsically scale with the square-root of brightness. **e)** The best-fit a_{fluc} values are shown (errorbars represent the 95% confidence interval of the curve fit). Statistical comparisons show that a_{fluc} is significantly higher for the for the fit to the high H-dimerization group (+H) than the low H-dimerization group (-H), indicating that the +H group is prone to a greater degree of intensity fluctuations (*** denotes $p<0.001$ and n.s. denotes $p>0.05$, calculated from the t-statistic of the best-fit confidence interval).

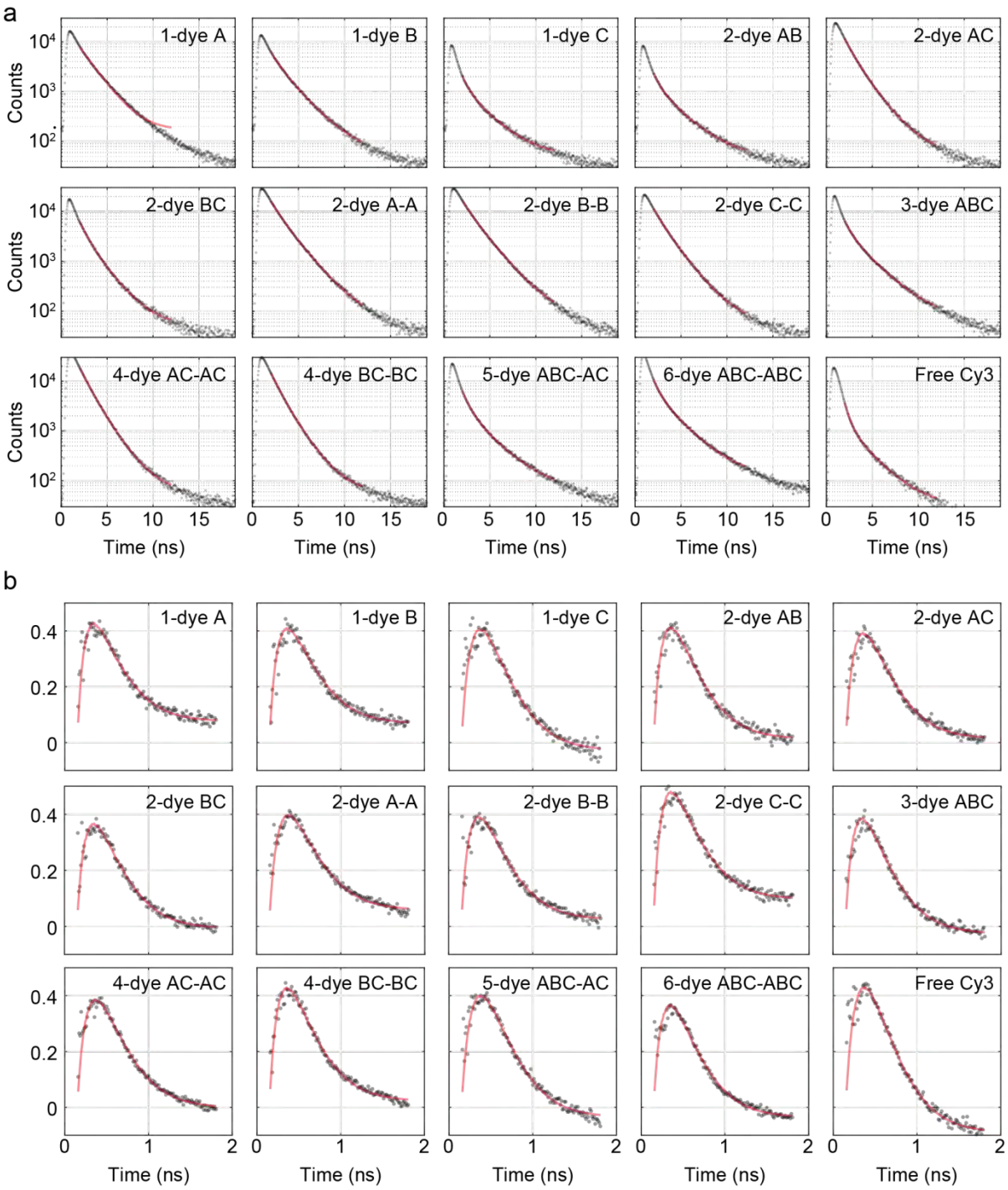

Figure S13: Fluorescence lifetime and time resolved fluorescence anisotropy curve fits
a) Each plot shows a representative histogram of photon arrival times (black dots) and a two-component exponential decay curve fit to the histogram tail (red) for a construct as noted in the plot. **b**) Each plot shows a representative average anisotropy vs. photon arrival time measurement (black dots) and a hindered rotor exponential decay curve fit with IRF deconvolution (red) for a construct as noted in the plot .

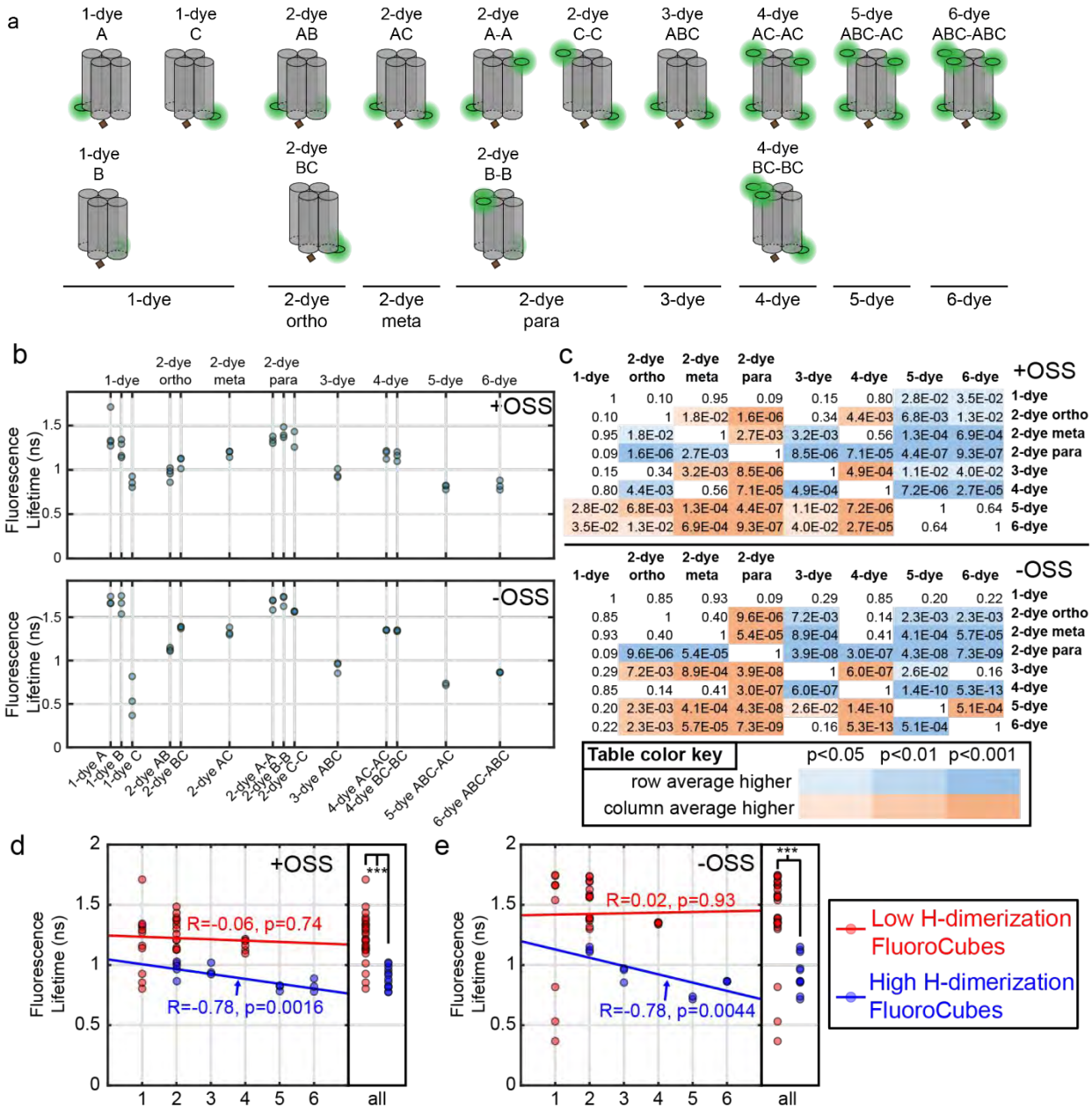

Figure S14: Comparison of fluorescence lifetime between groups of FluoroCube constructs
a) Illustrations of the 14 constructs used in this work, grouped. **b)** Two plots show data points (blue circles) from individual excited-state fluorescence lifetime measurements with (top) and without (bottom) OSS for each of the 14 constructs. Groups of constructs are clustered together. **c)** Tables of p-values from student's t-test comparisons between groups illustrated in corresponding plots in **b**. Each table entry shows the p-value for the comparison between the constructs indicated in the entry's row and column. Entries with p-values below 0.05 are colored according to the table shown on the bottom right. **d,e)** Trends of fluorescence lifetime with respect to *n* for constructs that do (blue) and don't (red) exhibit H-dimerization in the presence (**d**) and absence (**e**) of OSS and Trolox. Individual data points (circles) are shown with linear fits to the data points and are annotated with R and *p* values from Pearson's correlations (lines). The right side of each plot shows a t-test (***: $p<0.001$) between all measurements of H-dimerizing and non-H-dimerizing constructs.

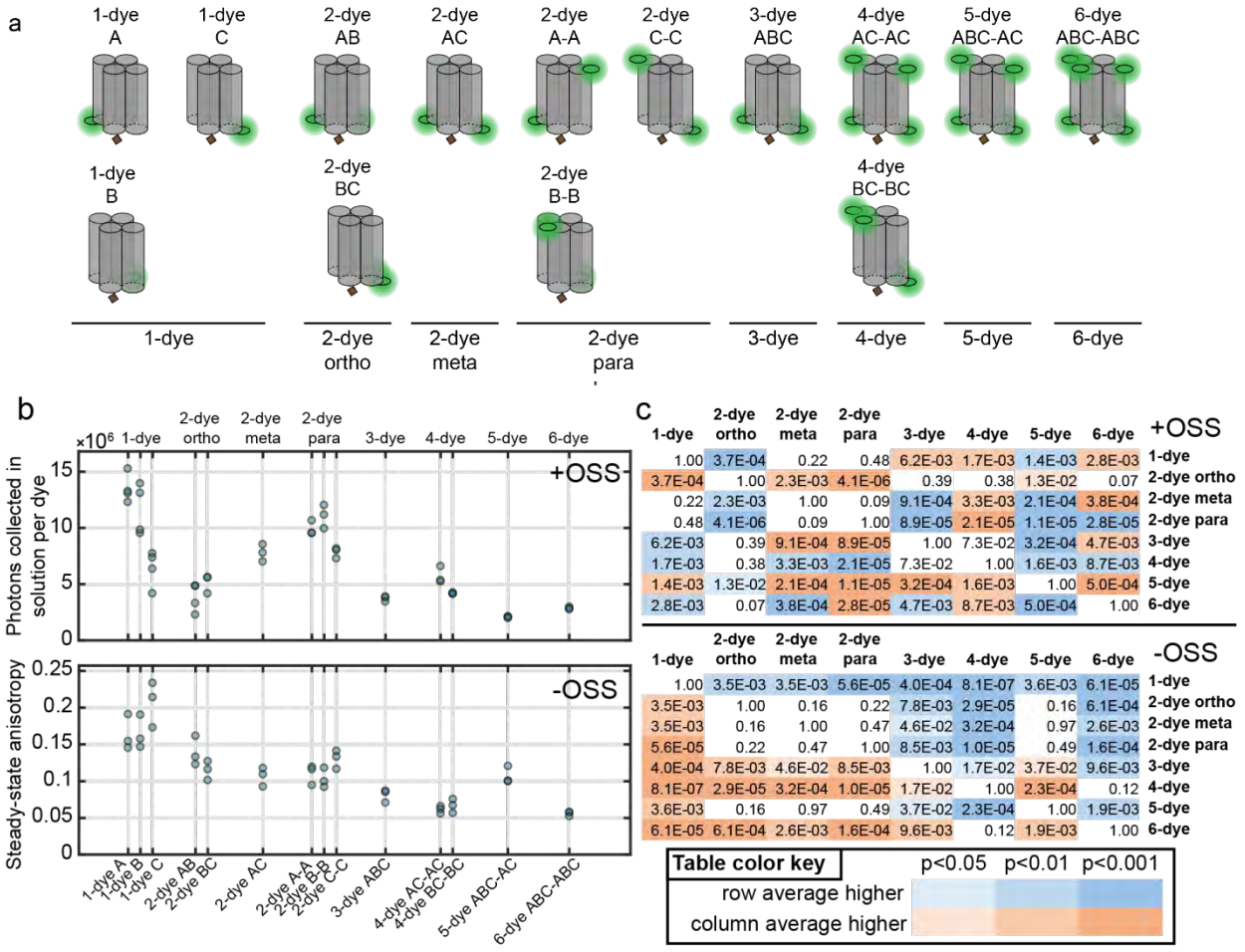

Figure S15: Comparison of photons collected per dye and between groups of FluoroCube constructs

a) Illustrations of the 14 constructs used in this work, grouped. **b)** Two plots show data points (blue circles) from individual measurements of the total number of photons (divided by n) detected during a fluorescence lifetime measurement with OSS (top) and the steady-state anisotropy measured without OSS (bottom) (+OSS measurements are shown in Figure S16) for each of the 14 constructs. Groups of constructs are clustered together. **c)** Tables of p-values from student's t-test comparisons between groups illustrated in corresponding plots in **b**. Each table entry shows the p-value for the comparison between the constructs indicated in the entry's row and column. Entries with p-values below 0.05 are colored according to the table shown on the figure's bottom right.

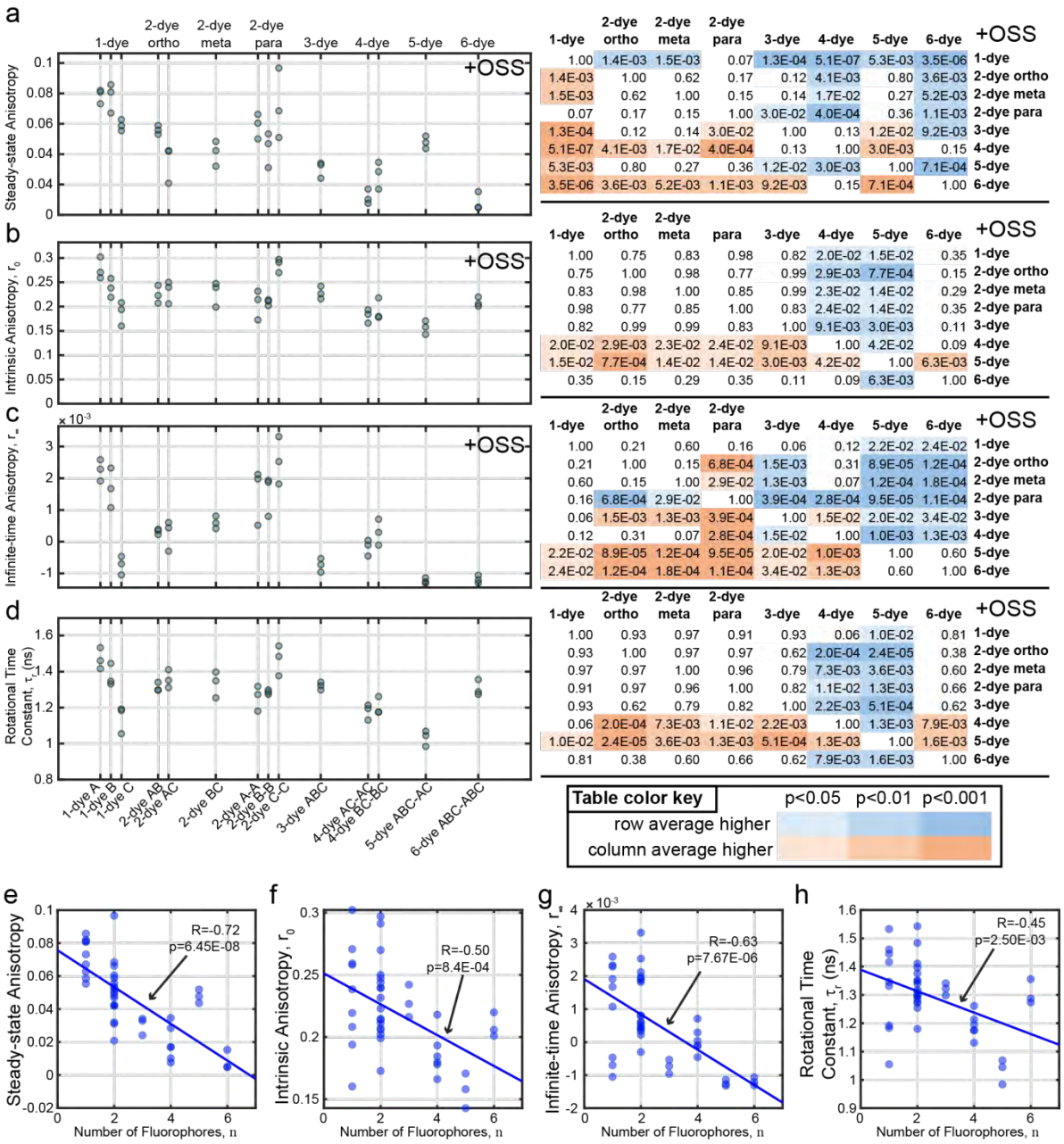

1-dye	2-dye ortho	2-dye meta	2-dye para	3-dye	4-dye	5-dye	6-dye	+OSS
1.00	1.4E-03	1.5E-03	0.07	1.3E-04	5.1E-07	5.3E-03	3.5E-06	1-dye
1.4E-03	1.00	0.62	0.17	0.12	4.1E-03	0.80	3.6E-03	2-dye ortho
1.5E-03	0.62	1.00	0.15	0.14	1.7E-02	0.27	5.2E-03	2-dye meta
0.07	0.17	0.15	1.00	3.0E-02	4.0E-04	0.36	1.1E-03	2-dye para
1.3E-04	0.12	0.14	3.0E-02	1.00	0.13	1.2E-02	9.2E-03	3-dye
5.1E-07	4.1E-03	1.7E-02	4.0E-04	0.13	1.00	3.0E-03	0.15	4-dye
5.3E-03	0.80	0.27	0.36	1.2E-02	3.0E-03	1.00	7.1E-04	5-dye
3.5E-06	3.6E-03	5.2E-03	1.1E-03	9.2E-03	0.15	7.1E-04	1.00	6-dye

1-dye	2-dye ortho	2-dye meta	para	3-dye	4-dye	5-dye	6-dye	+OSS
1.00	0.75	0.83	0.98	0.82	2.0E-02	1.5E-02	0.35	1-dye
0.75	1.00	0.98	0.77	0.99	2.9E-03	7.7E-04	0.15	2-dye ortho
0.83	0.98	1.00	0.85	0.99	2.3E-02	1.4E-02	0.29	2-dye meta
0.98	0.77	0.85	1.00	0.83	2.4E-02	1.4E-02	0.35	2-dye para
0.82	0.99	0.99	0.83	1.00	9.1E-03	3.0E-03	0.11	3-dye
2.0E-02	2.9E-03	2.3E-02	2.4E-02	9.1E-03	1.00	4.2E-02	0.09	4-dye
1.5E-02	7.7E-04	1.4E-02	1.4E-02	3.0E-03	4.2E-02	1.00	6.3E-03	5-dye
0.35	0.15	0.29	0.35	0.11	0.09	6.3E-03	1.00	6-dye

1-dye	2-dye ortho	2-dye meta	2-dye para	3-dye	4-dye	5-dye	6-dye	+OSS
1.00	0.21	0.60	0.16	0.06	0.12	2.2E-02	2.4E-02	1-dye
0.21	1.00	0.15	6.8E-04	1.5E-03	0.31	8.9E-05	1.2E-04	2-dye ortho
0.60	0.15	1.00	2.9E-02	1.3E-03	0.07	1.2E-04	1.8E-04	2-dye meta
0.16	6.8E-04	2.9E-02	1.00	3.9E-04	2.8E-04	9.5E-05	1.1E-04	2-dye para
0.06	1.5E-03	1.3E-03	3.9E-04	1.00	1.5E-02	2.0E-02	3.4E-02	3-dye
0.12	0.31	0.07	2.8E-04	1.5E-02	1.00	1.0E-03	1.3E-03	4-dye
2.2E-02	8.9E-05	1.2E-04	9.5E-05	2.0E-02	1.0E-03	1.00	0.60	5-dye
2.4E-02	1.2E-04	1.8E-04	1.1E-04	3.4E-02	1.3E-03	0.60	1.00	6-dye

1-dye	2-dye ortho	2-dye meta	2-dye para	3-dye	4-dye	5-dye	6-dye	+OSS
1.00	0.93	0.97	0.91	0.93	0.06	1.0E-02	0.81	1-dye
0.93	1.00	0.97	0.97	0.62	2.0E-04	2.4E-05	0.38	2-dye ortho
0.97	0.97	1.00	0.96	0.79	7.3E-03	3.6E-03	0.60	2-dye meta
0.91	0.97	0.96	1.00	0.82	1.1E-02	1.3E-03	0.66	2-dye para
0.93	0.62	0.79	0.82	1.00	2.2E-03	5.1E-04	0.62	3-dye
0.06	2.0E-04	7.3E-03	1.1E-02	2.2E-03	1.00	1.3E-03	7.9E-03	4-dye
1.0E-02	2.4E-05	3.6E-03	1.3E-03	5.1E-04	1.3E-03	1.00	1.6E-03	5-dye
0.81	0.38	0.60	0.66	0.62	7.9E-03	1.6E-03	1.00	6-dye

Figure S16 – Time resolved fluorescence anisotropy fit parameters correlate with n

a-d) Plots (left) show steady-state anisotropy or fit parameters r_0, τ_r, and r_∞ from individual time-resolved fluorescence anisotropy measurements (blue circles) with OSS and 30% glycerol for each of the 14 constructs. Groups of constructs are clustered together. Tables of p-values (right) from student's t-test comparisons between groups illustrated in corresponding plots on the left are also shown. Each table entry shows the p-value for the comparison between the constructs indicated in the entry's row and column. Entries with p-values below 0.05 are colored according to the table shown on the bottom right of **d**. **e-h)** Scatterplots of measurements from **a-d** plotted against n (blue circles) with a linear fit (blue), showing that all four parameters a significantly negatively correlated with n.

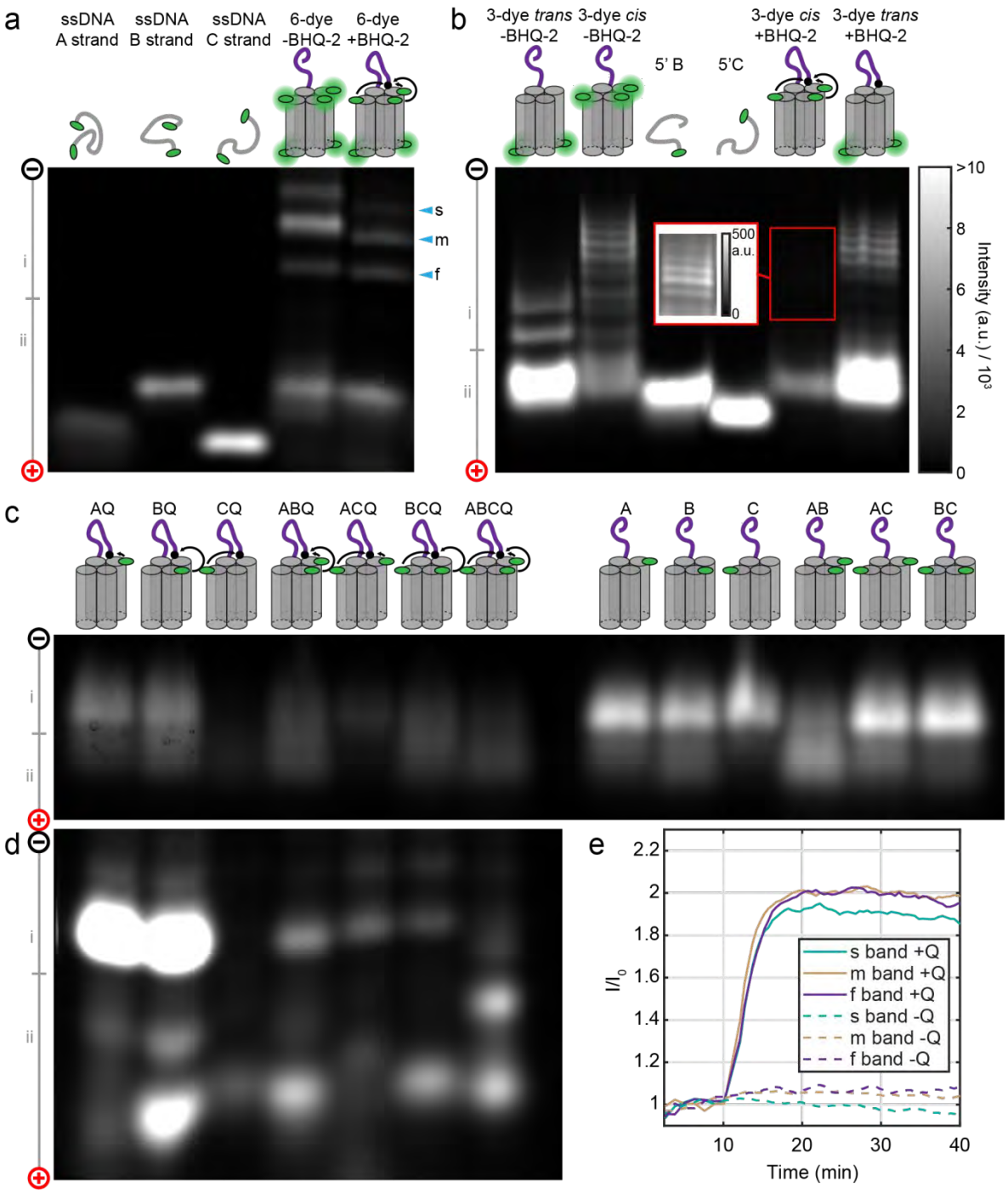

Figure S17: Fluorogenic FluoroCube constructs and purification

a-d) Schematic depictions and excerpts of Cy3 fluorescence images taken of agarose gels (3% agarose for 3 hours in **a-c**, 4% for 4.5 hours in **d**) post-electrophoresis for the fluorogenic constructs used in this work. All gel images are labeled on the left with a + and – end showing that the direction of electrophoretic flow was from top (-) to bottom (+) in the image. A dividing line shows the approximate flow coordinates that were generally interpreted as containing assembled FluoroCubes (i) or incomplete FluoroCubes and un-assembled single strands (ii). The construct (or single strand) in each lane is shown above in **a-c**, and the lanes in d correspond to lanes immediately above in **c** (the two gels were from different days with different FluoroCube assemblies, and the gel in **d** was imaged at higher resolution and run for 4.5 hrs instead of 3

hrs to achieve better separation between bands). All gel images were brightness adjusted to better show relevant gel bands. Due to efficient quenching of the *cis* 3-dye FluoroCube, a region of the gel in b is shown using a down-shifted intensity scale bar. Note that the 3-dye FluoroCubes shown in **b** were assembled from an early version of the single-dye strands that did not include 4T overhangs at their unlabeled termini, resulting in a high level of multimerization. **e)** A common feature of agarose gel electrophoresis results in this study is that assembled FluoroCubes often split into multiple bands. We expect that the lower mobility bands correspond to dimers, trimers, and higher order multimers that arise due to end-to-end stacking. To test whether these bands show similar results in our measurements of quenching efficiency, we isolated slow (s), medium (m), and fast (f) bands for FluoroCubes with and without quenchers as shown in subfigure **a**. In-solution fluorogenicity experiments shown in **e** suggest that the three bands display similar properties. These results suggest that multimers may form in the agarose gel and then separate when transferred to aqueous solution. As a result, most studies in this work incorporated FluoroCubes purified from a mixture of bands in region (i).

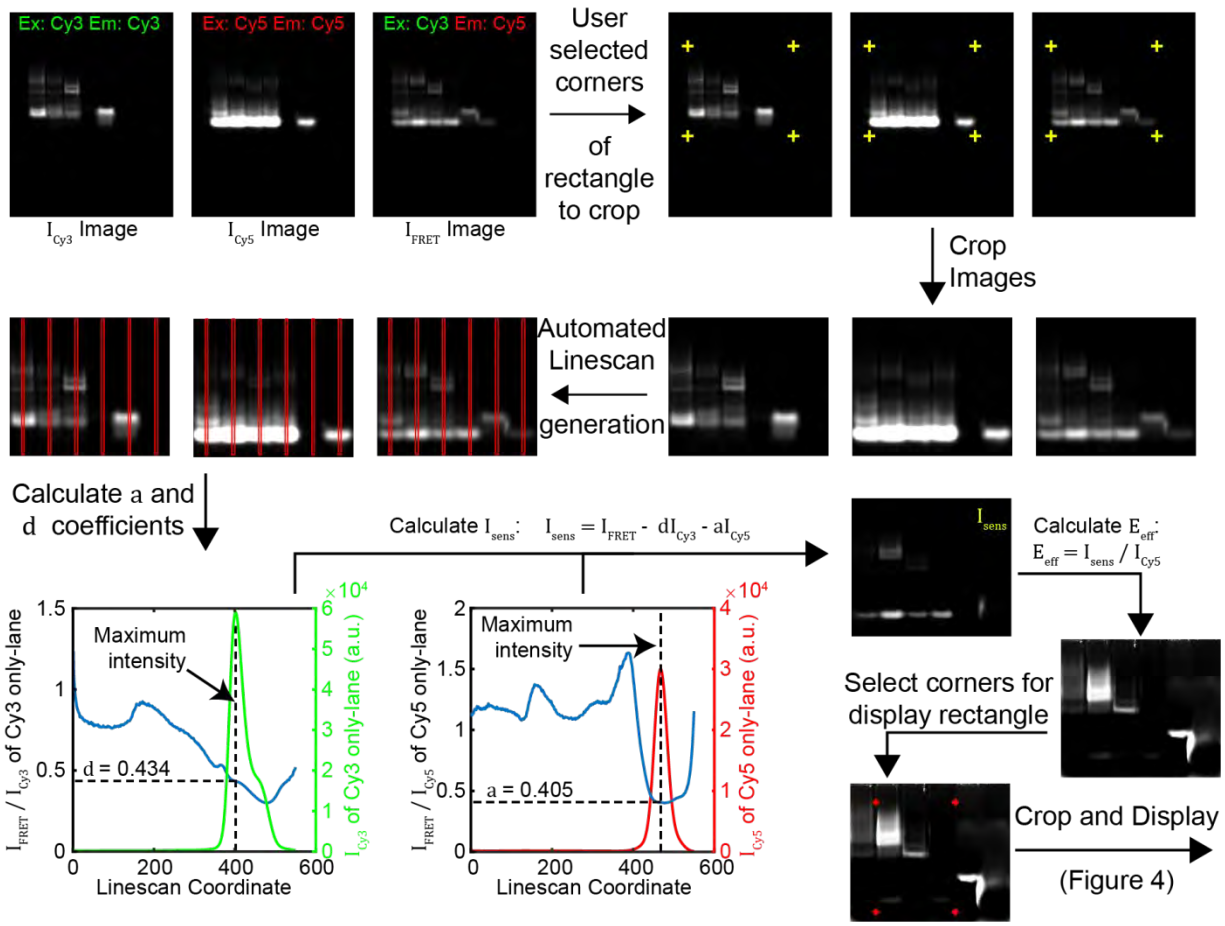

Figure S18: Image processing pipeline for FRET FluoroCube data

The image processing pipeline used to generate the data shown in Figures 4 and S19. Three raw fluorescence images (with excitation and emission colors denoted on each image) of agarose gels are shown on the top left. These images are then cropped via user annotation and linescans are taken from each lane. Six lanes are shown. Note that linescans run from top to bottom. The first lane (from the left) was not used in this work, while the second lane contains Cy3-Cy5 FluoroCube complexes, the third lane contains separated Cy3 and Cy5 FluoroCubes, the fourth lane contains FluoroCube complexes that lack Cy3 dyes, the fifth lane contains single-stranded Cy3-labeled strand, and the sixth lane contains single-stranded Cy5-labeled strands. To calculate E_{eff} in a pixel-by-pixel manner, the d parameter was calculated by measuring I_{FRET}/I_{Cy3} at the linescan position of peak intensity in the Cy3-only lane and the a parameter was calculated by measuring I_{FRET}/I_{Cy5} at the linescan position of peak intensity in the Cy5-only lane. I_{sens} and E_{eff} were then calculated using equations shown, and the image was further cropped for display in Figure 4. Note that bright regions in the Cy3-only lane (and in a small part of the separated complex lane) in the E_{eff} image are likely artifacts associated with the specific method for E_{eff} calculation used in this work.

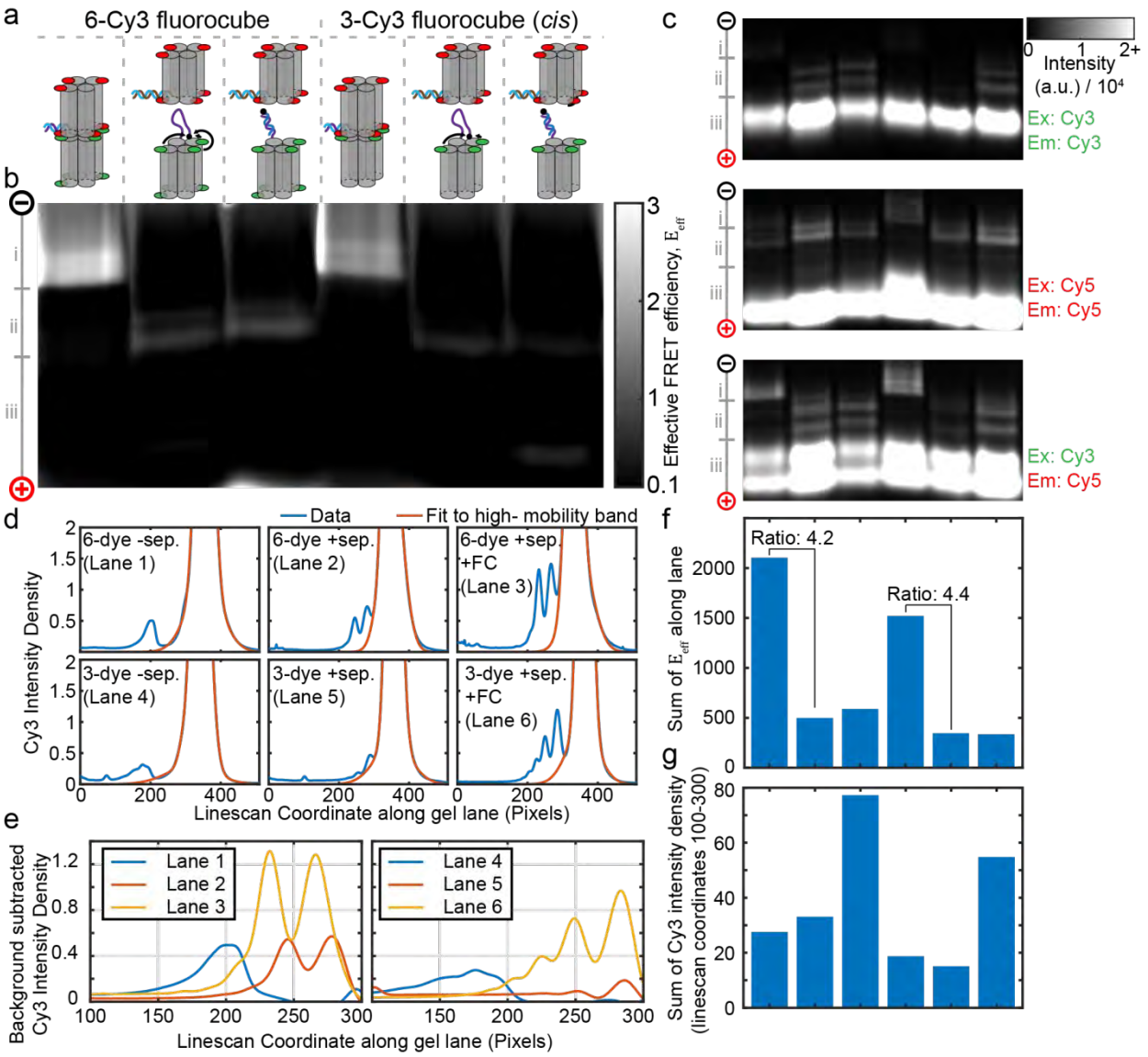

Figure S19: Replicate of FRET FluoroCube experiment

a) Schematics depictions of the components of the six lanes used for this experiment: FluoroCube complexes with 3-dye *cis* or 6-dye Cy3 fluorogenic FluoroCubes, as well as separated complexes in the presence or absence of a de-quenching strand. **b)** Image of the effective FRET efficiency E_{eff}, of single and complexed FluoroCubes (and fluorogenic FluoroCubes) in a 3% agarose gel after 3 hours of gel electrophoresis at 70 V. **c)** Raw images used to calculate E_{eff}. Gel images are labeled on the left with a + and – end showing that the direction of flow was from top (-) to bottom (+) in the image. Dividing lines shows the approximate coordinates that were generally interpreted as containing assembled FluoroCube complexes (i), individual FluoroCubes (ii), or incomplete FluoroCubes and un-assembled single strands (iii). **d)** Normalized intensity linescans of the six lanes (blue curves) with multi-Gaussian fits to the brightest, high mobility peak. These fits were used to remove the background intensity of the single stranded DNA. Fits for lanes [1, 2, 3, 4, 5, 6] were performed with [3, 3, 2, 4, 4, 4] Gaussians and starting from linescan coordinate [250 300 300 250 300 300]. Note that linescans run from top to bottom (i.e. linescan coordinate 0 corresponds to the top of the gel image, see Figure S18). Lanes are numbered from left to right. **e)** Background fit-subtracted linescans from coordinates 100-300 of each lane. For both 6-dye (left)

and 3-dye (right) Fluorocubes, the Cy3 intensity peak shifts rightward (i.e. higher mobility) upon FluoroCube complex separation, and then shifts slightly leftward (lower mobility) and upward (increased brightness) upon de-quenching – all in line with expectation. **f)** Integrated E_{eff} for the six lanes (this is mathematically valid because E_{eff} is proportional to the concentration of FRET complex) showing very high FRET for only the complexed FluoroCubes, and little-to-no difference between the quenched and un-quenched separated FluoroCubes. **g)** Integrated Cy3 intensity for the six linescans showing low intensity for the complexed and separated-but-quenched lanes, but high intensity for the separated unquenched lanes.

III. Supplementary Table 1 – Oligonucleotide sequences

Name	Sequence (5'-3')
Biotin strand	TACACATACTCATCCTACTACATCTCTCATCT/3Bio/
ssDNA strand	TACACATACTCATCCTACTACATCTCTCATCTTT**GCCTCATTATGTGCT**
BHQ-2 strand	TACACATACTCATCCTACTACATCTCTCATCTTT**GCCTCATTATGTGCT**/3BHQ_2/
Capture A	/5Biosg/TT TTT TTT TT TACACATACTCATCCTACTACATCTCTCATCT
Dual-Labeled A	/5Cy3/ATGAGGTGTATGTGTAGAGTGATGGATGTAGT/3Cy3Sp/
Dual-Labeled B	/5Cy3/AGGATGAGTGAGAGTGAGATGAGAGTAGATGT/3Cy3Sp/
Dual-Labeled C	/5Cy3/CACTCTCACACCTCATACATCTACCATCACTC/3Cy3Sp/
5'-Labeled A	/5Cy3/ATGAGGTGTATGTGTAGAGTGATGGATGTAGT TTTT
5'-Labeled B	/5Cy3/AGGATGAGTGAGAGTGAGATGAGAGTAGATGT TTTT
5'-Labeled C	/5Cy3/CACTCTCACACCTCATACATCTACCATCACTC TTTT
3'-Labeled A	TTTT ATGAGGTGTATGTGTAGAGTGATGGATGTAGT/3Cy3Sp/
3'-Labeled B	TTTT AGGATGAGTGAGAGTGAGATGAGAGTAGATGT/3Cy3Sp/
3'-Labeled C	TTTT CACTCTCACACCTCATACATCTACCATCACTC/3Cy3Sp/
Unlabeled A	TTTT ATGAGGTGTATGTGTAGAGTGATGGATGTAGT TTTT
Unlabeled B	TTTT AGGATGAGTGAGAGTGAGATGAGAGTAGATGT TTTT
Unlabeled C	TTTT CACTCTCACACCTCATACATCTACCATCACTC TTTT
Cy5 strand A	/5Cy5/GCAGAACACGCACACGAGACAGCAAGCACGAC/3Cy5Sp/
Cy5 strand B	/5Cy5/GAAGCAGACAGAGACAGAGCAGAGACGAGCAC/3Cy5Sp/
Cy5 strand C	/5Cy5/TGTCTCTGTGTTCTGCGTGCTCGTTGCTGTCT/3Cy5Sp/
Cy5 Pairing	ACTAT *AGCACATAATGAGGC* TT CGTGTGCGTCTGCTTCGTCGTGCTCTCTGCTC
Separator	**GCCTCATTATGTGCT** ATAGT
2-strand 2T	GAGTGATGTTGATGTAGTTTATGAGGTGTTTATGTGTATT/3Bio/
2-strand 4T	GAGTGATGTTTTGATGTAGTTTTTATGAGGTGTTTTTATGTGTATTTT/3Bio/
Fluorogenic ssDNA	/5Cy5/ **GCCTCATTATGTGCT**/3BHQ_2/
ssDNA complement	*AGCACATAATGAGGC*

The sequences are listed using Integrated DNA Technology (IDT)'s nomenclature. 3Bio and 5Bio = biotin ligated to the 3' and 5' termini, respectively. 5Cy3 and 3Cy3Sp = Cy3 ligated to 5' and 3' termini, respectively. 5Cy5 and 3Cy5Sp = Cy5 ligated to 5' and 3' termini, respectively. 3BHQ_2 = Black Hole Quencher 2 attached to the 3' DNA terminus. Underlined letters denote spacers. **Bold** segments are fully complementary to *italicized* segments.

IV. Supplementary Table 2 – List of oligonucleotide combinations comprising different types of FluoroCubes

Fluorocube Type	Ligand Strand	Strand A	Strand B	Strand C
6-dye Cy3	Biotin strand	Dual-Labeled A	Dual-Labeled B	Dual-Labeled C
3-dye ABC	Biotin strand	5'-Labeled A	3'-Labeled B	5'-Labeled C
1-dye A	Biotin strand	5'-Labeled A	Unlabeled B	Unlabeled C
1-dye B	Biotin strand	Unlabeled A	3'-Labeled B	Unlabeled C
1-dye C	Biotin strand	Unlabeled A	Unlabeled B	5'-Labeled C
2-dye AB	Biotin strand	5'-Labeled A	3'-Labeled B	Unlabeled C
2-dye AC	Biotin strand	5'-Labeled A	Unlabeled B	5'-Labeled C
2-dye BC	Biotin strand	Unlabeled A	3'-Labeled B	5'-Labeled C
2-dye A-A	Biotin strand	Dual-Labeled A	Unlabeled B	Unlabeled C
2-dye B-B	Biotin strand	Unlabeled A	Dual-Labeled B	Unlabeled C
2-dye C-C	Biotin strand	Unlabeled A	Unlabeled B	Dual-Labeled C
4-dye AC-AC	Biotin strand	Dual-Labeled A	Unlabeled B	Dual-Labeled C
4-dye BC-BC	Biotin strand	Unlabeled A	Dual-Labeled B	Dual-Labeled C
5-dye ABC-AC	Biotin strand	Dual-Labeled A	3' Labeled B	Dual-Labeled C
6-dye Cy5	Cy5 Pairing	Cy5 strand A	Cy5 strand B	Cy5 strand C
Fluorogenic 6-dye	BHQ-2 strand	Dual-Labeled A	Dual-Labeled B	Dual-Labeled C
Fluorogenic *cis* 3-dye	BHQ-2 strand	5'-Labeled A	3'-Labeled B	5'-Labeled C
Fluorogenic *trans* 3-dye	BHQ-2 strand	3'-Labeled A	5'-Labeled B	3'-Labeled C
Fluorogenic 1-dye A	BHQ-2 strand	5'-Labeled A	Unlabeled B	Unlabeled C
Fluorogenic 1-dye B	BHQ-2 strand	Unlabeled A	3'-Labeled B	Unlabeled C
Fluorogenic 1-dye C	BHQ-2 strand	Unlabeled A	Unlabeled B	5'-Labeled C
Fluorogenic 2-dye AB	BHQ-2 strand	5'-Labeled A	3'-Labeled B	Unlabeled C
Fluorogenic 2-dye AC	BHQ-2 strand	5'-Labeled A	Unlabeled B	5'-Labeled C
Fluorogenic 2-dye BC	BHQ-2 strand	Unlabeled A	3'-Labeled B	5'-Labeled C

6-dye no BHQ-2	ssDNA strand	Dual-Labeled A	Dual-Labeled B	Dual-Labeled C
cis 3-dye no BHQ-2	ssDNA strand	5'-Labeled A	3'-Labeled B	5'-Labeled C
trans 3-dye no BHQ-2	ssDNA strand	3'-Labeled A	5'-Labeled B	3'-Labeled C
1-dye A no BHQ-2	ssDNA strand	5'-Labeled A	Unlabeled B	Unlabeled C
1-dye B no BHQ-2	ssDNA strand	Unlabeled A	3'-Labeled B	Unlabeled C
1-dye C no BHQ-2	ssDNA strand	Unlabeled A	Unlabeled B	5'-Labeled C
2-dye AB no BHQ-2	ssDNA strand	5'-Labeled A	3'-Labeled B	Unlabeled C
2-dye AC no BHQ-2	ssDNA strand	5'-Labeled A	Unlabeled B	5'-Labeled C
2-dye BC no BHQ-2	ssDNA strand	Unlabeled A	3'-Labeled B	5'-Labeled C
2-dye 2-strand 2T	2-strand 2T	Dual-Labeled A		
2-dye 2-strand 4T	2-strand 4T	Dual-Labeled A		
1-dye 2-strand 4T	2-strand 4T	5'-Labeled A		
1-dye dsDNA	5'-Labeled A	Capture A		

V. Supplemental Note 1

Starting from equation (2) in the main text:

$$f = 1 - (1 - \exp(-k_1 t))^n$$

τ can be solved for by setting $f = 1/2$ and $t = \tau$ and re-arranging:

$$\frac{1}{2} = 1 - (1 - \exp(-k_1 \tau))^n$$

$$\frac{1}{2} = (1 - \exp(-k_1 \tau))^n$$

$$\left(\frac{1}{2}\right)^{\frac{1}{n}} = 1 - \exp(-k_1 \tau)$$

$$\exp(-k_1 \tau) = 1 - \left(\frac{1}{2}\right)^{\frac{1}{n}}$$

$$-k_1 \tau = \ln\left(1 - 2^{\frac{-1}{n}}\right)$$

$$\tau = -\frac{\ln\left(1 - 2^{\frac{-1}{n}}\right)}{k_1}$$

For low n values (i.e. ≤ 6 used in this study), this curve can be accurately approximated (<1.1% relative error, (true-approx)/true – see the figure below) using a simplified expression that is used in the main text:

$$\tau \approx \frac{1.13 \ln(n+1)}{k_1}$$

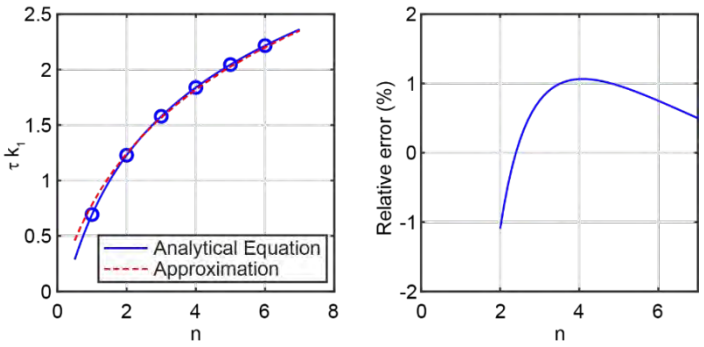

VI. Supplemental Note 2

To assess whether 4-dye FluoroCubes are more likely to exist as multimers (i.e., multiple FluoroCubes attached to each other) during single molecule photobleaching studies, we analyzed the histograms of the number of photons detected per FluoroCube in the first frame for 4-dye AC-AC, 4-dye BC-BC, and 6-dye FluoroCubes (see figure below, left side). The presence of a substantial population of multimers would result in a positive skewness (a measure of a distribution's asymmetry, with positive skewness indicating a tail on the right side of the distribution) in the initial photon count population (because multimers should emit, 2×, 3×, 4×, etc. as many photons as monomeric FluoroCubes). We used 1,000 iterations of bootstrapping to measure the 95% confidence interval of the skewness of each histogram and found that the 95% confidence interval of the 6-dye FluoroCube population skewness overlaps with the skewness of both types of 4-dye FluoroCubes (and vice-versa). Therefore, we find no statistically significant evidence of increased multimerization by 4-dye FluoroCubes.

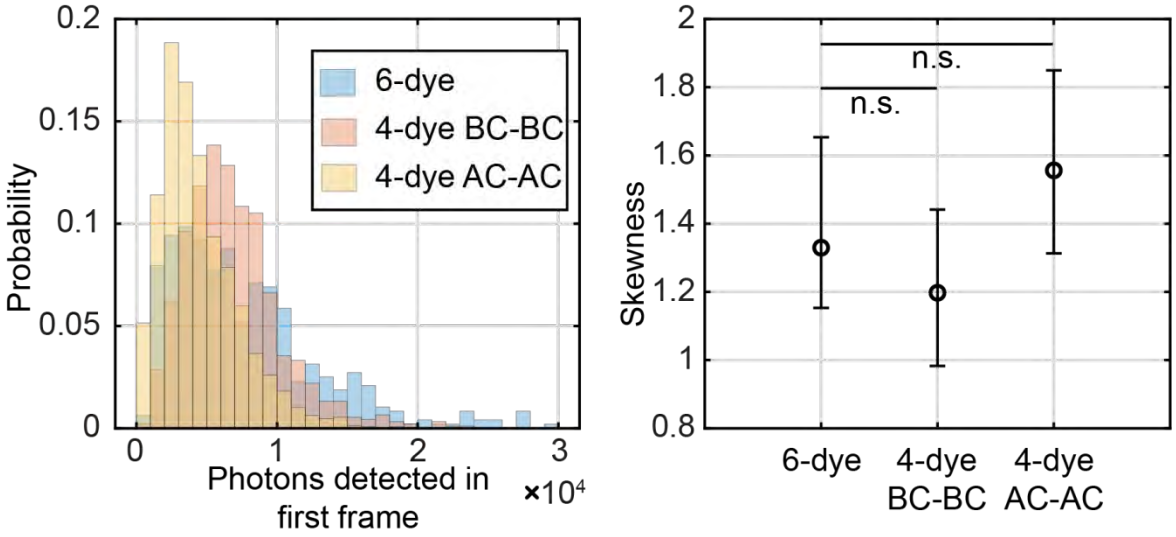

As a second means of showing that 4-dye FluoroCubes do not multimerize more than 6-dye FluoroCubes do, we took linescans of 4-dye, 5-dye, and 6-dye FluoroCubes in agarose gel lanes (Figure S1 – linescan taken from top to bottom). The 6-dye FluoroCubes were run on a different gel and imaged with higher resolution than the other FluoroCubes, so we normalized each linescan to the maximum intensity and scaled the linescan along the linescan coordinate (see below figure) until the two main peaks (corresponding to assembled and unassembled FluoroCubes) approximately overlapped. Visual inspection of the normalized linescans reveals no substantial difference between the left shoulders of the assembled FluoroCube peaks, suggesting that there is no observable difference in multimerization between 4-, 5-, and 6-dye FluoroCubes.

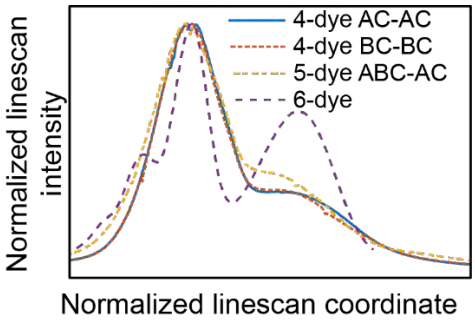

VII. Supplemental Note 3

To better understand the extent to which dye-dye interactions affect FluoroCube performance, we analyzed our single molecule photobleaching results based on relative dye positioning. To accomplish this, we first grouped FluoroCube constructs into eight groups depending on FluoroCube positioning (Figure S8-9): 1-dye; 2-dye *ortho*, wherein two dyes are positioned on neighboring duplexes; 2-dye meta, wherein two dyes are positioned on the same side of the FluoroCube on non-neighboring duplexes (i.e., diagonally); 2-dye *para*, wherein two dyes are positioned on opposite sides of the FluoroCube; 3-dye; 4-dye; 5-dye; and 6-dye. We then compared $N_{photons}$, k_1, and first-frame brightness (I_0) between these groups in the presence (Figure S8) and absence (Figure S9) of OSS. This analysis revealed very few significant differences in k_1 between groups, suggesting that k_1 is largely independent of inter-dye spacing. We also observed few differences in $N_{photons}$ between groups with $n > 3$ and between groups with $n \leq 3$. The same bifurcation was observed for first-frame brightness in the absence of OSS. However, in the presence of OSS, first-frame brightness was more graded: 1-dye ≈ all 2-dye groups < 3-dye < 5-dye ≈ 6-dye < 4-dye. The lack of substantial differences between 2-dye groups suggests that inter-dye spacing alone is not determinative of intensity-altering dye-dye interactions under these conditions. However, the general sub-linear scaling of FluoroCube brightness with n still suggests that dye-dye interactions are important.

VIII. Supplemental Note 4

Beyond H-dimerization, we hypothesized that additional interactions between dyes in weak coupling range (~2-6 nm) could be meaningful. To evaluate the extent to which energy transfer occurs between Cy3 molecules, we measured the steady-state fluorescence anisotropy of all fourteen constructs (Figure S15). Fluorescence anisotropy is a measure of the alignment of the polarization of excitation and emission light, and is typically interpreted (for single-dye molecular structures) as inversely correlating to the fluorophore's rotational mobility. Since the Cy3 fluorophores in all constructs are attached to the same DNA nanostructure, we do not expect differences in rotational mobility between constructs. However, for multi-fluorophore systems such as FluoroCubes, decreased fluorescence anisotropy is a sign of homoFRET (FRET between pairs of Cy3 dyes), because the transition dipole moments of dyes undergoing homoFRET do not necessarily have to be well-aligned. We observed a nearly monotonic decrease in fluorescence anisotropy with respect to n (Figure S15c), suggesting that the degree of homoFRET increases with the number of dyes. We found no effect of inter-dye spacing on fluorescence anisotropy for 2-dye constructs (p>0.05, Figure S15c), suggesting that the rate of homoFRET is roughly similar between all pairs of dyes on the FluoroCube.

To better understand the role of homoFRET, we analyzed the time-resolved nature of our fluorescence anisotropy measurements by fitting average anisotropy, $r(t)$, vs. arrival time, t, curves with the equation

$$r(t) = (r_0 - \mathrm{r}_\infty)\exp\left(t/\tau_r\right) + r_\infty\#$$

where r_0 is the intrinsic anisotropy (Figure S16a, the fluorescence anisotropy as the time between emission and excitation approaches the limit of zero), r_∞ is the baseline anisotropy (which is positive when fluorophores cannot freely rotate to all orientations) and τ_r is the time constant of anisotropy decay. The steady-state anisotropy is simply the time average of $r(t)$. Interestingly, τ_r, r_0, and r_∞ all exhibited significant negative correlations with n. The slight decrease of τ_r with increasing n suggests that homoFRET increases the rate of realignment of the excited state (e.g., due to homoFRET between imperfectly-aligned dyes) on a timescale that is close to the dyes' fluorescence lifetimes (~1 ns). The nonzero (although very small) values of r_∞ at low n suggest that individual dyes can undergo confined local rotation but, consistent with other studies of dyes coupled to DNA origami nanostructures[6], the FluoroCube does not rotate freely within the lifetime of the fluorophores. The negative correlation between r_∞ and n suggests that homoFRET expands the orientational space that the excited state can occupy before emission. Finally, the negative correlation between r_0 and n suggests that there may also be energy transfer processes that occur on timescales that are too fast to detect using our instrumentation (sub ~100 ps).

HomoFRET alone is not expected to substantially affect FluoroCube function because limited energy is lost during energy transfer. HomoFRET from non-H-dimerizing dyes to H-dimerizing dyes could more significantly reduce brightness by funneling energy towards energy-sinks (H-dimers). Moreover, the occurrence of homoFRET suggests that singlet-singlet annihilation, which occurs through a similar resonance energy mechanism as homoFRET, may play an important role in FluoroCube function.[7,8] Specifically, singlet-singlet annihilation occurs when two fluorophores on the same FluoroCube are in the excited state at once. The two excited dyes electronically couple, resulting in non-radiative de-excitation of both dyes. Because the excited state lifetime is only 1-2 ns, co-excitation of multiple dyes within such a short time window only occurs at high laser power. Therefore, singlet-singlet annihilation is expected to result in a sub-linear relationship between brightness and excitation laser power – a result that was previously observed[1]. Supporting this previous finding, we find that the number of photons detected per dye decreased significantly with n – even for non-H-dimerizing FluoroCubes – during our fluorescence lifetime measurement, which was performed using a confocal microscope that excites fluorophores with relatively high power density (~8,000 W/cm^2) (Figure S15d). In contrast, our single molecule photobleaching experiment, which was performed on a widefield TIRF microscope with comparatively low

excitation power density (~8 W/cm^2), did not exhibit this negative correlation between $N_{photons}/n$ and n for constructs with low degrees of H-dimerization (Figure S11). These results suggest that FluoroCubes are preferentially suited for lower power density applications (e.g., widefield, TIRF, particle tracking, STORM, lightsheet) when compared to higher power density applications (e.g., confocal imaging, STED, fluorescence correlation spectroscopy).

IX. References

1 Niekamp, S., Stuurman, N. & Vale, R. D. A 6-nm ultra-photostable DNA FluoroCube for fluorescence imaging. *Nat. Methods* **17**, 437-441, doi:10.1038/s41592-020-0782-3 (2020).

2 Johnson-Buck, A. *et al.* Kinetic fingerprinting to identify and count single nucleic acids. *Nat. Biotechnol.* **33**, 730-732, doi:10.1038/nbt.3246 (2015).

3 Khanna, K. *et al.* Rapid kinetic fingerprinting of single nucleic acid molecules by a FRET-based dynamic nanosensor. *Biosens. Bioelectron.* **190**, 113433, doi:https://doi.org/10.1016/j.bios.2021.113433 (2021).

4 Hayward, S. L. *et al.* Ultraspecific and Amplification-Free Quantification of Mutant DNA by Single-Molecule Kinetic Fingerprinting. *J. Am. Chem. Soc.* **140**, 11755-11762, doi:10.1021/jacs.8b06685 (2018).

5 Crocker, J. C. & Grier, D. G. Methods of Digital Video Microscopy for Colloidal Studies. *J. Colloid Interface Sci.* **179**, 298-310, doi:https://doi.org/10.1006/jcis.1996.0217 (1996).

6 Mathur, D. *et al.* Can a DNA Origami Structure Constrain the Position and Orientation of an Attached Dye Molecule? *The Journal of Physical Chemistry C* **125**, 1509-1522, doi:10.1021/acs.jpcc.0c09258 (2021).

7 Schröder, T., Scheible, M. B., Steiner, F., Vogelsang, J. & Tinnefeld, P. Interchromophoric Interactions Determine the Maximum Brightness Density in DNA Origami Structures. *Nano Lett.* **19**, 1275-1281, doi:10.1021/acs.nanolett.8b04845 (2019).

8 Hofkens, J. *et al.* Revealing competitive Förster-type resonance energy-transfer pathways in single bichromophoric molecules. *Proc. Natl. Acad. Sci. U. S. A.* **100**, 13146, doi:10.1073/pnas.2235805100 (2003).